Preprint typeset in JHEP style - HYPER VERSION

AP-GR-109
OCU-PHYS-401
OU-HET-819
RIKEN-MP-91

arXiv:1407.0798v1 [hep-th] 3 Jul 2014

Electric Field Quench in AdS/CFT

Koji Hashimoto[1,2], **Shunichiro Kinoshita**[3], **Keiju Murata**[4] **and Takashi Oka**[5]

[1] *Department of Physics, Osaka University, Toyonaka, Osaka 560-0043, Japan*
[2] *Mathematical Physics Lab., RIKEN Nishina Center, Saitama 351-0198, Japan*
[3] *Osaka City University Advanced Mathematical Institute, Osaka 558-8585, Japan*
[4] *Keio University, 4-1-1 Hiyoshi, Yokohama 223-8521, Japan*
[5] *Department of Applied Physics, University of Tokyo, Tokyo 113-8656, Japan*

E-mails: koji@phys.sci.osaka-u.ac.jp, kinosita@sci.osaka-cu.ac.jp, keiju@phys-h.keio.ac.jp, oka@ap.t.u-tokyo.ac.jp

Abstract: An electric field quench, a suddenly applied electric field, can induce non-trivial dynamics in confining systems which may lead to thermalization as well as a deconfinement transition. In order to analyze this nonequilibrium transitions,we use the AdS/CFT correspondence for $\mathcal{N} = 2$ supersymmetric QCD that has a confining meson sector. We find that the electric field quench causes the deconfinement transition even when the magnitude of the applied electric field is smaller than the critical value for the static case (which is the QCD Schwinger limit for quark-antiquark pair creation). The time dependence is crucial for this phenomenon, and the gravity dual explains it as an oscillation of a D-brane in the bulk AdS spacetime. Interestingly, the deconfinement time takes only discrete values as a function of the magnitude of the electric field. We advocate that the new deconfinement phenomenon is analogous to the exciton Mott transition.

Keywords: AdS/CFT, Deconfinement, Thermalization, Electric field.

Contents

1. Introduction: Time-dependent electric field and deconfinement **2**

2. A review of static embeddings with electric fields **5**
- 2.1 Basic equation 5
- 2.2 Observables in the boundary theory 6
- 2.3 Effective metric and horizon 6
- 2.4 Boundary conditions at effective horizon and pole 7
- 2.5 Brane solutions 8

3. Dynamics of D7-brane with electric fields **9**
- 3.1 Basic equations 9
- 3.2 Observables at the AdS boundary 12
- 3.3 Boundary conditions 13
- 3.4 Initial data 13

4. Thermalization and deconfinement in dynamical systems **15**
- 4.1 Definition of deconfinement 16
- 4.2 Definition of thermalization 18

5. Results for supercritical electric fields **19**
- 5.1 Brane motion and boundary observable 19
- 5.2 Thermalization and deconfinement time 20

6. Results for subcritical electric fields **22**
- 6.1 Quark condensate and electric current 22
- 6.2 Deconfinement below the critical electric field 24

7. Conclusion and discussions **29**

A. Equations of motion from the DBI action **32**

B. $d \neq 0$ cases **34**

C. Stark effect for scalar and vector mesons **35**

D. Error analysis **36**

1. Introduction: Time-dependent electric field and deconfinement

Obviously one of the most important unanswered question in QCD is the mechanism of quark confinement. Experimentally, RHIC experiments and subsequent LHC experiments created a deconfined phase of QCD by heavy ion collisions, which have provided us a new perspective of the deconfinement transition. However, the cause of deconfinement is still a mystery, mainly because we do not know the mechanism of the confinement.

To reach the deconfined phase, we need some external force put into the system. Heavy ion experiments have two aspects, one is the temperature raise caused by the thermalized gluons and the other is the strong electromagnetic fields created right after the impact of ions [1–5]. A high temperature is sufficient for the deconfinement as lattice simulations of QCD suggest, while putting strong electric field can make the QCD vacuum unstable against a creation of quark-antiquark pairs, known as Schwinger mechanism, which also leads to deconfinement.

The obstacle in theoretical analysis for this issue of the mechanism of the deconfinement transition is apparently the strong coupling and non-perturbative nature of QCD. During the last decade, the AdS/CFT correspondence [6–8] turned out to be a useful tool for calculating strongly-coupled gauge theory analytically. The virtue of the AdS/CFT correspondence is that it can be applied also to time-dependent system, as opposed to lattice QCD simulations.

In this paper, we demonstrate an AdS/CFT analysis of an "electric field quench" — a sudden apply of an electric field — for a strongly coupled gauge theory.[1] Figure 1 shows the characteristic profile of a time-dependent electric field; starting originally from zero, it is turned on with a ramp followed by a constant value. The profile is a smeared step function whose height is E_f and the duration of the ramp is parametrized by a time period ΔV.

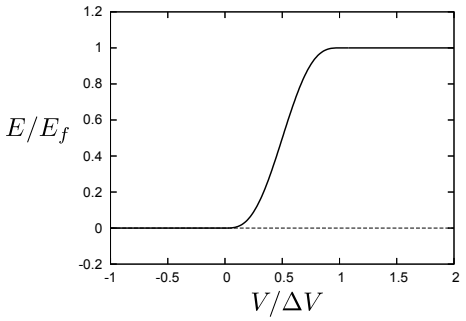

Figure 1: The profile of the external electric field applied to the system, $E(V)$. V is the time coordinate.

We shall study the simplest toy model of strongly coupled gauge theory in string theory, namely the $\mathcal{N} = 2$ $SU(N_c)$ supersymmetric QCD at large N_c and at strong coupling. The theory has an $\mathcal{N} = 4$ supersymmetric Yang-Mills (gluonic) sector and an $\mathcal{N} = 2$ quark hypermultiplet [22]. When the quark has a mass, the meson spectrum is discrete, while the gluon sector is completely deconfined. So this serves as a toy model for a quark "confinement" occurring only in the meson sector. The behavior of the system under an external electric field can be studied by analyzing the dynamics of the probe flavor D7-brane in the $AdS_5 \times S^5$ geometry. It is known

[1] Some AdS/CFT examples of quantum quenches of quark sectors are found in [9–11]. On the other hand, thermalization due to a quantum quench on gluonic sector in AdS/CFT were popularly studied (see for example Refs. [12–21]).

that, in the static case, there exists a critical electric field $E_{\rm crit}$ beyond which the phase transition occurs. Beyond the critical electric field $E > E_{\rm crit}$, the confinement is broken and there appears an electric current carried by the quarks [23–25].[2] However, below the critical electric field $E < E_{\rm crit}$, the system is still a confined phase for mesons.

Interestingly, we find that even if the magnitude of the electric field is below the critical electric field, we can reach the deconfinement phase once we apply it in a time-dependent manner. See our result, Fig. 15. The lines in Fig. 15 divide the $(\Delta V, E_f)$-plane into two regions — the upper-left region is a parameter region which leads to the deconfinement. Notice that even for small final value of the electric field E_f, if the duration ΔV is sufficiently short, we can reach the deconfinement. Our result would imply a novel mechanism which may be working at heavy ion collisions: the electric field caused by the fast ions can help the deconfinement transition even if the magnitude of the electric field is small compared to the QCD scale.

Furthermore, we find a strange behavior of the deconfinement timescale: The calculated deconfinement time takes only discrete values, as a function of the magnitude of the final electric field E_f for a fixed ΔV. See the result shown in Fig. 12.

Here we briefly describe what is happening in the gravity dual picture to reach the conclusions described above. The AdS/CFT correspondence can make the detailed calculation possible in a time-dependent manner. In the gravity dual, after turning on the electric field, the D7-brane moves in the bulk $\mathrm{AdS}_5 \times S^5$ geometry. See Fig. 2 for an illustration of the D7-brane motion in the $\mathrm{AdS}_5 \times S^5$ spacetime. The motion looks like an oscillation, since the external input changes only the boundary behavior of the D7-brane, and the boundary motion propagates into the bulk motion on the D7-brane. The energy pumped into the D7-brane will create a strongly red-shifted region on the D7-brane, which is an indication of the deconfinement in the gravity side. We find that even if the magnitude of the oscillation is small, if the energy is pumped in a short duration, the red-shifted region on the D7-brane emerges. That is the reason why we can make the deconfinement even with small magnitude of the electric field.

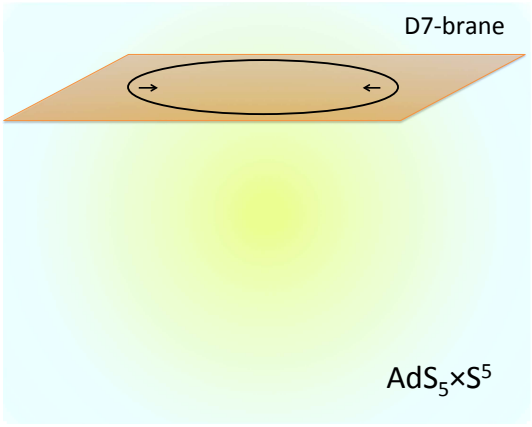

Figure 2: A schematic picture of a D7-brane in the $\mathrm{AdS}_5 \times S^5$ geometry. The D7-brane is shown as a square flat surface. If we turn on the external electric field, the fluctuation wave on the D7-brane comes in from the boundary. The wave is shown as a circle shrinking on the D7-brane.

[2]Supercritical electric fields can make the QCD vacuum unstable against Schwinger pair production of quarks. See [26, 27] for the evaluation of the Euler-Heisenberg Lagrangian and the instability associated with the imaginary part of the effective action. See also [28–39] for AdS/CFT calculations of the Schwinger production.

Since the D7-brane fluctuation in the AdS_5 space is similar to a wave in a finite-sized box, the oscillation caused at the boundary propagates into the bulk but after a while it is reflected back to the boundary. Repeating this reflection sharpens the wave packet and finally creates a naked singularity which causes a strongly red-shifted region on the D7-brane. The number of reflections depends on parameters E_f and ΔV. The reflection takes place at a multiple of time necessary for the wave to propagate from the boundary to the center of the bulk on the D7-brane. So, the deconfinement time is discretized from the gravity viewpoint. However, how to interpret the AdS/CFT result in the gauge theory side is nontrivial.

In any time-dependent set-up, giving a proper definition of the "deconfinement" and the "thermalization" is a nontrivial issue. In this paper, we propose a new definition which is universal for any gravity dual setups. *We define the deconfinement time as the time when the redshift factor becomes very large. Furthermore, we define the thermalization as the time when the redshift factor grows exponentially.* We are interested in the D7-brane meson sector, so we calculate the redshift factor of an effective metric on the D7-brane. There are several reasons for the usefulness of these definitions. First, if the event horizon is formed, inside of the event horizon and itself cannot be known by the boundary observer, while the redshift factor can be measured. Secondly, apparent horizons, which are commonly used for a definition of the thermalization in AdS/CFT, will not always emerge outside of the event horizon and they can not capture the universal features of thermalization for wider gravity duals. Thirdly, the new definition is directly related to spectrum of the Hawking radiation to be observed by the boundary observer and reduces to the standard Hawking thermal temperature for static cases.

The organization of our paper is as follows. After giving a brief review on the flavor D7-brane embedding in the $AdS_5 \times S^5$ geometry for the static case in section 2, we provide our description of the time-dependent D-brane motion in section 3. We explain our coordinate system and the equations of motion, and the profile of the time-dependent external electric field and the AdS/CFT dictionary to extract the physical observables. In section 4, we provide careful definitions of the deconfinement and the thermalization: the deconfinement is defined as the emergence of a strong redshift factor for the D-brane effective metric, and the thermalization is defined as a slow settlement of the Hawking temperature given by the effective metric. Later sections are for the presentation of our numerical results. First, in section 5, we show the thermalization and the deconfinement for the applied electric field which is greater than the critical value. In section 6, we analyze the case with the electric field smaller than the critical value, and we find that the deconfinement still takes place. We show that deconfinement time takes only discrete values, and explains the reason from the AdS bulk viewpoint. Section 7 is devoted for a conclusion and discussions.

2. A review of static embeddings with electric fields

2.1 Basic equation

In this section, we briefly review results of static embeddings with electric fields living on the D7-brane [23–25]. We consider $AdS_5 \times S^5$ spacetime as the background solution:

$$ds^2 = \frac{L^2}{z^2}\left[-dV^2 - 2dVdz + dx_1^2 + dx_2^2 + dx_3^2\right] + L^2(d\phi^2 + \cos^2\phi d\Omega_3^2 + \sin^2\phi d\psi^2) \ , \tag{2.1}$$

where L is the AdS radius. Although one can use the ordinary time coordinate $dt = dV + dz$ instead of V in static cases, we take the ingoing Eddington-Finkelstein coordinates for convenience of later dynamical calculations. The embeddings of D7-brane are described by the Dirac-Born-Infeld (DBI) action,

$$S = -\mu_7 g_s^{-1}\int d^8\sigma\sqrt{-\det[h_{ab} + 2\pi\alpha' F_{ab}]} \ , \tag{2.2}$$

where $\mu_7 = (2\pi)^{-7}\alpha'^{-4}$ and g_s is the string coupling. h_{ab} is the brane induced metric, which is defined by $h_{ab} = g_{\mu\nu}\partial_a X^\mu \partial_b X^\nu$. Here X^μ is the brane collective coordinate and $g_{\mu\nu}$ is the metric in the target space. F_{ab} is the field strength on the brane worldvolume, which is defined by $F_{ab} = \partial_a A_b - \partial_b A_a$. As the worldvolume coordinates, we use the target space coordinates themselves as $\{\sigma^a\} = (V, z, \Omega_3, \vec{x}_3)$. Assuming time translational symmetry generated by ∂_V, spherical symmetry of S^3, translational symmetries generated by $(\partial_{x_1}, \partial_{x_2}, \partial_{x_3})$, and rotational symmetry on (x_2, x_3)-plane, the brane position and gauge potential are written as

$$\phi = \Phi(z) \ , \quad \psi = 0, \quad 2\pi\alpha' L^{-2} A_a d\sigma^a = \{-EV + a(z)\}dx_1 \ . \tag{2.3}$$

In this paper, since we will not take account of finite baryon number density in the boundary theory, we have omitted the V-components of the gauge potential, $a_V(z)dV$. For static embeddings with non-zero baryon number density, see in [23, 44, 45]. Note that while the gauge potential contains a time dependent component, $-EVdx_1$, the field strength is time independent and this term gives a constant external electric field along x_1-direction in the boundary theory. Because of the symmetry generated by ∂_ψ in the background spacetime, we set $\psi = 0$ without loss of generality. Then, the DBI action is written as

$$\begin{aligned} S &= -\mu_7 g_s^{-1} V_4 \Omega_3 L^8 \int dz \frac{\cos^3\Phi(z)}{z^5}\sqrt{\xi} \ , \\ \xi &\equiv z^2\bar{F}(z)\Phi'(z)^2 + z^4\{a'(z)^2 + 2Ea'(z)\} + 1 \ , \end{aligned} \tag{2.4}$$

where $V_4 \equiv \int dV dx_1 dx_2 dx_3$, $\Omega_3 = \mathrm{Vol}(S^3) = 2\pi^2$ and $\bar{F}(z) \equiv 1 - E^2 z^4$. Equations of motion for $a(z)$ and $\Phi(z)$ are given as

$$\frac{\cos^3\Phi}{z\sqrt{\xi}}(a' + E) = j \ , \quad \left(\frac{\bar{F}\cos^3\Phi}{z^3\sqrt{\xi}}\Phi'\right)' + \frac{3\sin\Phi\cos^2\Phi}{z^5}\sqrt{\xi} = 0 \ . \tag{2.5}$$

Since the action only depends on a' but does not contain a explicitly, we have obtained the conservation law as the first equation. The constant of motion j will be related to the electric current in the boundary theory. From the first equation in Eq. (2.5), we have

$$\xi = \frac{\bar{F}(1+z^2\Phi'^2)\cos^6\Phi}{-j^2z^6+\cos^6\Phi} \ . \tag{2.6}$$

Substituting the above equation into the second equation of Eq. (2.5), we obtain a single equation for Φ as

$$\begin{aligned}\Phi'' = \frac{1}{2z^8\bar{F}(-j^2+z^{-6}\cos^6\Phi)}\Big[&-6\bar{F}\sin\Phi\cos^5\Phi(1+z^2\Phi'^3) \\ &- z^4\{\cos^6\Phi(\bar{F}'-8z^{-1}\bar{F}) - j^2z^6(\bar{F}'-2z^{-1}\bar{F})\}\Phi'^3 \\ &- z^2\{\cos^6\Phi(\bar{F}'-6z^{-1}\bar{F}) - j^2z^6\bar{F}'\}\Phi'\Big] \ . \end{aligned} \tag{2.7}$$

In practical numerical calculations, introducing a new variable $W(z) = z^{-1}\sin\Phi(z)$, we solve the equation for $W(z)$ obtained by rewriting the above equation in term of $W(z)$.

2.2 Observables in the boundary theory

Near the AdS boundary $z = 0$, solutions are expanded as

$$\frac{1}{z}\sin\Phi(z) = m + cz^2 + \cdots \ , \quad a(z) = -Ez + \frac{j}{2}z^2 + \cdots \ . \tag{2.8}$$

One can easily check that the expansion coefficient j coincides with the constant of motion appeared in Eq. (2.5). The constants m, E, c and j correspond to quark mass m_q, electric field $\mathcal{E}$, quark condensate $\langle\mathcal{O}_m\rangle$, and electric current $\langle J^x\rangle$ as

$$\begin{aligned} m_q &= \frac{L^2m}{2\pi\alpha'} = \left(\frac{\lambda}{2\pi^2}\right)^{1/2} m \ , \qquad \mathcal{E} = \frac{L^2E}{2\pi\alpha'} = \left(\frac{\lambda}{2\pi^2}\right)^{1/2} E \ , \\ \langle\mathcal{O}_m\rangle &= -\frac{N_c\sqrt{\lambda}}{2^{3/2}\pi^3}\, c \ , \qquad \langle J^x\rangle = \frac{N_c\sqrt{\lambda}}{2^{5/2}\pi^3}\, j \ , \end{aligned} \tag{2.9}$$

where λ denotes the 't Hooft coupling. Ignoring proportional constants, we will refer to m, E, c and j themselves as quark mass, electric field, quark condensate and electric current, hereafter.

2.3 Effective metric and horizon

In appendix A, we show that the embedding functions of the brane, which describe the brane position in the target space, and the gauge field on the brane are governed by non-linear wave equations on the following effective metric:

$$\gamma_{ab} = h_{ab} + (2\pi\alpha')^2 h^{cd}F_{ac}F_{bd} \ . \tag{2.10}$$

Therefore, causality for fluctuations propagating on the brane is determined by this effective metric [45, 48–51]. Substituting our ansatz (2.3), we obtain the effective metric for the static embedding as

$$L^{-2}\gamma_{ab}d\sigma^a d\sigma^b = -\frac{\bar{F}}{z^2}dV^2 - \frac{2}{z^2}(1+Ez^4a')dVdz + (\Phi'^2 + z^2a'^2)dz^2 \\ + \frac{z^2\bar{F}\Phi'^2 + z^4a'(a'+2E)+1}{z^2(1+z^2\Phi'^2)}dx_1^2 + \frac{1}{z^2}(dx_2^2+dx_3^2) + \cos^2\Phi d\Omega_3^2 \ . \quad (2.11)$$

This metric is manifestly singular at $\Phi(z) = \pi/2$, at which the radius of S^3 wrapped by the brane goes to zero. Thus, the domain of the z-coordinate is given by $0 \leq z \leq z_{\rm max}$ where $\Phi(z_{\rm max}) = \pi/2$. The event horizon (Killing horizon) in this metric will appear at $z = E^{-1/2} \equiv z_{\rm eff}$, where $\bar{F}(z_{\rm eff}) = 0$, if $z_{\rm eff} < z_{\rm max}$. We refer to the surface $z = z_{\rm eff}$ as the effective horizon. Note that the effective horizon is different from bulk event horizon in general. In fact, although the background spacetime is now pure AdS without any black hole and just the Cauchy horizon is located at $z = \infty$, the effective horizon can emerge on the D-brane at $z = z_{\rm eff}$. Furthermore, the effective horizon is time-like in the view of the bulk metric and can be seen from the AdS boundary through the bulk null geodesic.

Based on the effective metric, we can define effective surface gravity. A Killing vector $\xi_a = (\partial_V)_a$ is the null generator of the effective horizon. The effective surface gravity κ is defined by $\xi^b\hat{D}_b\xi_a|_{z=z_{\rm eff}} = -\kappa\xi_a|_{z=z_{\rm eff}}$ where $\hat{D}$ is the covariant derivative with respect to γ_{ab}. From Eq. (2.11), we obtain

$$\kappa = \frac{2E^{3/2}}{E + a'(z_{\rm eff})} \ , \quad (2.12)$$

Quanta of brane fluctuations are emitted from the vicinity of the effective horizon as Hawking radiation with the temperature $\kappa/(2\pi)$.[3]

2.4 Boundary conditions at effective horizon and pole

We can consider two kinds of static embeddings depending on values of $z_{\rm eff}$ and $z_{\rm max}$. When the effective horizon does not emerge on the brane ($z_{\rm eff} > z_{\rm max}$), the D7-brane solution is called a *Minkowski embedding*. In this case, the brane reaches the pole ($\Phi = \pi/2$) at which the S^3 shrinks to zero. Now, the first equation in (2.5) can be rewritten as

$$\frac{\cos^6\Phi}{z^2}(a'+E)^2 = j^2[z^4(a'+E)^2 + \bar{F}(z)(1+z^2\Phi'^2)]. \quad (2.13)$$

For the Minkowski embeddings, since $\cos\Phi = 0$ should be satisfied at the pole $z = z_{\rm max}$, we have $j = 0$ from the above equation. Furthermore, from the regularity

[3]For massless case $m = 0$, the effective temperature is studied in more general set up in Ref. [46].

of Eq. (2.7), asymptotic solution near the pole becomes

$$W(z) = \frac{1}{z_{\rm max}} - \frac{E^2 z_{\rm max}^2}{2 - E^2 z_{\rm max}^4}(z - z_{\rm max}) + \cdots \ , \tag{2.14}$$

which gives us a boundary condition for the Minkowski embeddings.

When the effective horizon emerges on the brane ($z_{\rm eff} < z_{\rm max}$), the D7-brane solution is called a *black hole embedding*. In this case, since $\bar{F}(z_{\rm eff}) = 0$ at the effective horizon, (2.13) leads to

$$j = \frac{\cos^3 \Phi(z_{\rm eff})}{z_{\rm eff}^3} \ . \tag{2.15}$$

Here, we have assumed $a'(z_{\rm eff}) + E \neq 0$. Otherwise we obtain $a' + E \sim \sqrt{z_{\rm eff} - z}$ which results in a singular behavior of a'' at the effective horizon. Thus, (2.15) is a natural condition derived by the equation of motion for the gauge field.[4] From the regularity of Eq. (2.7), asymptotic solution near the effective horizon becomes

$$W(z) = W_{\rm eff} - \frac{1 - (1 - W_{\rm eff}^2 z_{\rm eff}^2)^{1/2}}{W_{\rm eff} z_{\rm eff}^3}(z - z_{\rm eff}) + \cdots \ . \tag{2.16}$$

where $W_{\rm eff} \equiv W(z_{\rm eff}) = \sin \Phi(z_{\rm eff})/z_{\rm eff}$.

2.5 Brane solutions

Using Eqs. (2.14) or (2.16) as the boundary condition, we solve Eq. (2.7) from the pole or the effective horizon to the AdS boundary $z = 0$. In Fig. 3, we show profiles of the D7-brane in the unit of $E = 1$. As the vertical and the horizontal axes, we have taken Cartesian-like coordinates $(w, \rho) = (z^{-1} \sin \phi, z^{-1} \cos \phi)$. In the (w, ρ)-plane, the effective horizon is shown by an unit circle, $w^2 + \rho^2 = 1$.

From these solutions, we can read off the quark condensate c and electric current j. In Fig. 4(a) and (b), we plot the c and j as functions of electric field E. They are normalized by the quark mass m.[5] (Quark condensate $c(E)$ and electric current $j(E)$ were computed explicitly in Refs. [24,25] and Ref. [47], respectively.) They take multiple values in $0.5754 < E/m^2 < 0.5766$. This indicates that there is a phase transition between Minkowski and black hole embeddings. In fact, in Refs. [24, 25], they found a first-order phase transition at $E/m^2 = 0.57588$ by a thermodynamical argument. We show the transition point by a vertical line in the figure. The quark condensate and electric current make finite jump between points A and B. Note that,

[4]Note that it relates to imposing the reality condition of the D-brane action [23–25, 43] such that the denominator of Eq. (2.6) must change the sign at the effective horizon where $\bar{F}$ changes the sign.

[5]Throughout this paper, we will nondimensionalize variables by quark mass m unless otherwise noted.

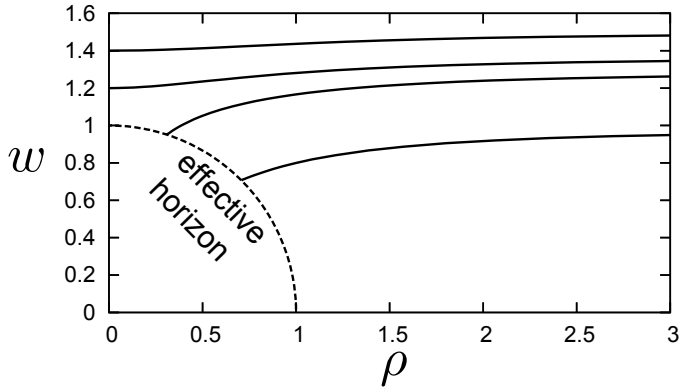

Figure 3: Minkowski and black hole embeddings of D7-brane in the unit of $E = 1$. The effective horizon is located at $z = 1$ which is shown by an unit circle in this figure.

for $E/m^2 < 0.5754$, we obtain only Minkowski embeddings and, thus, the electric current is exactly zero. For black hole embeddings, the differential resistance dj/dE can be negative as pointed out in Ref. [47].

For pure AdS background, the effective surface gravity is simply written as

$$\kappa = [3E(1 + E^{1/2} j^{-1/3})]^{1/2} \ , \tag{2.17}$$

where we used Eqs. (2.5), (2.6), (2.12) and (2.15). Since we have already computed the electric current j as a function of E, we can easily obtain the the effective surface gravity as in Fig. 4(c). At the point where both Minkowski and black hole embeddings join, κ diverges. For $0.5754 < E/m^2 < 0.724$, the surface gravity can be a decreasing function of the electric field E. It takes minimum value at $(E/m^2, \kappa/m) = (0.724, 2.527)$ and, for $E/m^2 > 0.724$, increases monotonically. For strong electric field $E/m^2 \gg 1$, we have $\Phi(z_{\rm eff}) \simeq 0$. Thus, we obtain $j \simeq z_{\rm eff}^{-3} = E^{-3/2}$ from Eq. (2.15). Therefore, for strong limit of the electric field, we have analytical expression the the surface gravity as $\kappa \simeq (6E)^{1/2}$.

3. Dynamics of D7-brane with electric fields

In this paper, we study far-from-equilibrium dynamics of $\mathcal{N} = 2$ supersymmetric QCD, which is induced by time dependent external electric fields. We will turn on a homogeneous electric field from zero to finite non-zero value and examine the response of the system. This means we should deal with dynamics of the D7-brane and the gauge field living on the brane. In this section, we explain our model and formulation for solving the dynamics numerically.

3.1 Basic equations

We use the $\mathrm{AdS}_5 \times S^5$ spacetime (2.1) as the background, which means that we focus on zero temperature for the bulk gluon. The dynamics of the D7-brane is

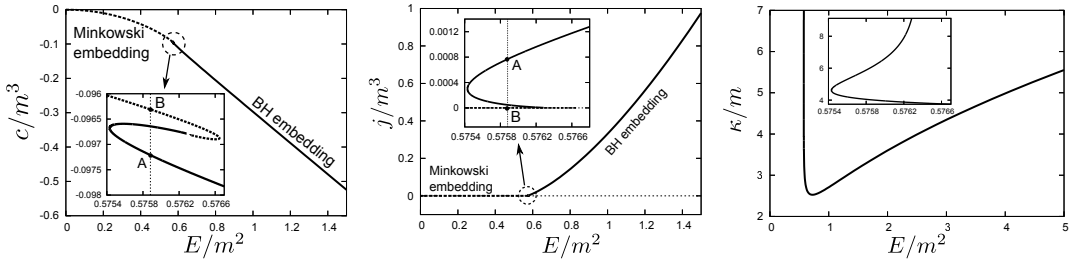

(a) quark condensate (b) electric current (c) effective surface gravity

Figure 4: Quark condensate c, electric current j and effective surface gravity κ for the static embeddings. The quark condensate and the electric current make finite jump between the points A and B by the first-order phase transition. The effective surface gravity takes minimum value at $(E/m^2, \kappa/m) = (0.724, 2.527)$.

described by the DBI action (2.2). Hereafter, we take the unit where the AdS radius is unity, $L = 1$.

We introduce eight worldvolume coordinates $\{\sigma^a\}$ $(a = 0, 1, \cdots, 7)$ on the brane. For six of them, we use the target space coordinates themselves as $(\sigma^2, \cdots, \sigma^7) = (\vec{x}_3, \Omega_3)$. For the other two coordinates, we introduce (u, v)-coordinates which are determined by imposing coordinate conditions later. Imposing spherical symmetry of S^3, translational symmetries generated by $(\partial_{x_1}, \partial_{x_2}, \partial_{x_3})$, and rotational symmetry on (x_2, x_3)-plane, the brane collective coordinates and the gauge potential are written as

$$\begin{aligned} &V = V(u, v) \ , \quad z = Z(u, v) \ , \quad \phi = \Phi(u, v) \ , \quad \psi = 0 \ , \\ &2\pi\alpha' A_a d\sigma^a = a_u(u, v)du + a_v(u, v)dv + a_x(u, v)dx_1 \ . \end{aligned} \tag{3.1}$$

Note that, since (x_2, x_3)-components of the gauge potential are absent, we will denote x_1-component of that as a_x briefly. Here, because of the $U(1)$-symmetry generated by ∂_ψ, we can set $\psi = 0$ without loss of generality.

Then, the D7-brane action is written as

$$\begin{aligned} &S = -\mu_7 g_s^{-1} V_3 \Omega_3 \int du dv \frac{\cos^3\Phi}{Z^3}\sqrt{\xi} \ , \\ &\xi \equiv -f_{uv}^2 + (h_{uv} + Z^2\partial_u a_x \partial_v a_x)^2 - (h_{uu} + Z^2\partial_u a_x^2)(h_{vv} + Z^2\partial_v a_x^2) \end{aligned} \tag{3.2}$$

where $V_3 \equiv \int dx_1 dx_2 dx_3$, $\Omega_3 = \mathrm{Vol}(S^3) = 2\pi^2$, and

$$\begin{aligned} &f_{uv} = \partial_u a_v - \partial_v a_u \ , \quad h_{uv} = -Z^{-2}(V_{,u}V_{,v} + V_{,u}Z_{,v} + V_{,v}Z_{,u}) + \Phi_{,u}\Phi_{,v} \ , \\ &h_{uu} = -Z^{-2}V_{,u}(V_{,u} + 2Z_{,u}) + \Phi_{,u}^2 \ , \quad h_{vv} = -Z^{-2}V_{,v}(V_{,v} + 2Z_{,v}) + \Phi_{,v}^2 \ . \end{aligned} \tag{3.3}$$

From equations of motion for a_u and a_v, we obtain

$$\frac{\cos^3\Phi}{Z^3\sqrt{\xi}} f_{uv} = d \ , \tag{3.4}$$

where d is an integration constant corresponding to the baryon number density in the boundary theory. In this paper, we focus on zero baryon number density and assume $d = 0$, namely $f_{uv} = 0$, hereafter. (For general cases see appendix B.)

Now, since the action has coordinate freedom of (u, v)-coordinates, we can take a convenient coordinate system for numerically solving dynamics. As we mentioned, dynamics of the D-brane and the gauge field on the brane are governed by wave equations on the effective metric. In order to introduce double-null coordinate system in two-dimensional part of the effective metric, we impose coordinate conditions:

$$C_1 \equiv h_{uu} + Z^2(\partial_u a_x)^2 = 0 \ , \tag{3.5}$$

$$C_2 \equiv h_{vv} + Z^2(\partial_v a_x)^2 = 0 \ , \tag{3.6}$$

which are double-null conditions for the effective metric rather than the induced metric. Indeed, under these coordinate conditions, the effective metric is written as

$$\begin{aligned}\gamma_{ab}d\sigma^a d\sigma^b = 2(h_{uv} + Z^2 f_{ux}f_{vx})dudv \\ + \frac{1}{Z^2}\frac{h_{uv} + Z^2 f_{ux}f_{vx}}{h_{uv} - Z^2 f_{ux}f_{vx}}dx_1^2 + \frac{1}{Z^2}d\vec{x}_2^2 + \cos^2\Phi d\Omega_3^2 \ ,\end{aligned} \tag{3.7}$$

where the effective metric is defined by Eq. (2.10). Note that these coordinate conditions are constraint equations.

Then, the square root in the DBI action (3.2) can be removed and the action is simply written as

$$S = \mu_7 g_s^{-1} V_3 \Omega_3 \int dudv \frac{\cos^3\Phi}{Z^3}(h_{uv} + Z^2 \partial_u a_x \partial_v a_x). \tag{3.8}$$

Deviating this action, we can obtain evolution equations for V, Z, Φ and a_x. For convenience in numerical calculations we introduce a new variable instead of $\Phi(u, v)$ as

$$\Psi(u, v) \equiv \frac{\Phi(u, v)}{Z(u, v)} \ . \tag{3.9}$$

In term of the variables (V, Z, Ψ, a_x), the evolution equations are written as

$$\begin{aligned}V_{,uv} = \frac{3}{2}Z(Z\Psi)_{,u}(Z\Psi)_{,v} + \frac{3}{2}\tan(Z\Psi)\{(Z\Psi)_{,u}V_{,v} + (Z\Psi)_{,v}V_{,u}\} \\ - \frac{5}{2Z}V_{,u}V_{,v} + \frac{Z^3}{2}a_{x,u}a_{x,v} \ ,\end{aligned} \tag{3.10}$$

$$\begin{aligned}Z_{,uv} = -\frac{3}{2}Z(Z\Psi)_{,u}(Z\Psi)_{,v} + \frac{3}{2}\tan(Z\Psi)\{(Z\Psi)_{,u}Z_{,v} + (Z\Psi)_{,v}Z_{,u}\} \\ + \frac{5}{2Z}(V_{,u}V_{,v} + V_{,u}Z_{,v} + V_{,v}Z_{,u}) + \frac{5}{Z}Z_{,u}Z_{,v} - \frac{Z^3}{2}a_{x,u}a_{x,v} \ ,\end{aligned} \tag{3.11}$$

$$\Psi_{,uv} = \frac{3}{2}\left(\Psi + \frac{\tan(Z\Psi)}{Z}\right)(Z\Psi)_{,u}(Z\Psi)_{,v}$$

$$+\frac{1}{2Z^2}\{1-3Z\Psi\tan(Z\Psi)\}\{(Z\Psi)_{,u}Z_{,v}+(Z\Psi)_{,v}Z_{,u}\}$$
$$-\frac{\Psi}{2Z^2}\left(5-\frac{3\tan(Z\Psi)}{Z\Psi}\right)(V_{,u}V_{,v}+V_{,u}Z_{,v}+V_{,v}Z_{,u})$$
$$-\frac{3\Psi}{Z^2}Z_{,u}Z_{,v}+\frac{Z^2\Psi}{2}\left(1-\frac{3\tan(Z\Psi)}{Z\Psi}\right)a_{x,u}a_{x,v}\ , \qquad (3.12)$$

$$a_{x,uv}=\frac{3}{2}\tan(Z\Psi)\{(Z\Psi)_{,u}a_{x,v}+(Z\Psi)_{,v}a_{x,u}\}+\frac{1}{2Z}(Z_{,u}a_{x,v}+Z_{,v}a_{x,u})\ . \qquad (3.13)$$

They guarantee that the coordinate conditions (3.5) and (3.6) are preserved in the time evolutions as

$$\partial_u\Big[\frac{\cos^3\Phi}{Z^5}C_2\Big]=\partial_v\Big[\frac{\cos^3\Phi}{Z^5}C_1\Big]=0\ . \qquad (3.14)$$

Therefore, once we have imposed the coordinate conditions as initial conditions and boundary conditions, $C_1 = 0$ and $C_2 = 0$ are automatically satisfied and we only have to solve the evolution equations.

It turns out that the form of the equations of motion is quite similar to that in Ref [11] except for the gauge field a_x. Since a stable numerical method to solve this kind of equations has been developed there, we will follow the numerical method to solve Eqs. (3.10)-(3.13) and skip detail explanations of the numerics in this paper.

3.2 Observables at the AdS boundary

Eliminating u and v, we can regard Ψ and a_x as functions of V and Z. Near the AdS boundary $Z = 0$, these functions are expanded as

$$\Psi(V,Z)=m+\left(c(V)+\frac{m^3}{6}\right)Z^2+\cdots\ , \qquad (3.15)$$

$$a_x(V,Z)=\alpha_0(V)+\dot{\alpha}_0(V)Z+\frac{1}{2}j(V)Z^2+\frac{1}{2}\ddot{\alpha}_0(V)Z^2\ln(mZ)+\cdots\ . \qquad (3.16)$$

It is convenient to rewrite the leading term of a_x as

$$\alpha_0(V)\equiv-\int^V dV'E(V')\ . \qquad (3.17)$$

Here, m, $E(V)$, $c(V)$ and $j(V)$ are related to quark mass, electric field, quark condensate and electric current in the boundary theory as in Eq. (2.9). Once we give the leading terms m and $E(V)$ as boundary conditions for Ψ and a_x, we can determine $c(V)$ and $j(V)$ by solving the evolution equations. In our following calculations, we choose a C^2 function for $E(V)$ as

$$E(V)=\begin{cases}0 & (V<0)\\ E_f[V-\frac{\Delta V}{2\pi}\sin(2\pi V/\Delta V)]/\Delta V & (0\le V\le\Delta V)\\ E_f & (V>\Delta V)\end{cases}\ , \qquad (3.18)$$

where E_f is a final value of the electric field and ΔV is a rise time taken from zero electric field to the final one. The profile of the function $E(V)$ is shown in Fig. 1.

3.3 Boundary conditions

In general, two time-like boundaries will appear in numerical domain on the brane worldvolume: one is the AdS boundary $Z = 0$, and the other is the pole $\Phi = \pi/2$ at which the radius of S^3 wrapped by the D7-brane shrinks to zero. For numerical convenience, we should fix the location of each boundary in the worldvolume (u, v)-coordinates if the numerical domain contains that boundary. Note that coordinate conditions (3.5) and (3.6) are invariant under the residual coordinate transformations,

$$\bar{u} = \bar{u}(u) \ , \qquad \bar{v} = \bar{v}(v) \ , \tag{3.19}$$

which generate a conformal transformation in the two-dimensional spacetime. Using them, we can fix the location of the AdS boundary and the pole on the worldvolume coordinates as $u = v$ and $u = v + \pi/2$, respectively. In Fig. 5, we show our computational domain in (u, v)-plane.

Since we are interested in time evolutions on the AdS boundary, the AdS boundary is always contained in the numerical domain and located at $u = v$ throughout our calculations. Boundary conditions at the AdS boundary for Z, Ψ and a_x are determined by asymptotic behaviors (3.15) and (3.16) as $Z|_{u=v} = 0$, $\Psi|_{u=v} = m$ and $a_x|_{u=v} = \alpha_0(V)$. That is, we consider the quark mass is fixed at a non-zero value and the electric field is time-dependent in the boundary theory. We can derive the condition for V from regularities of the evolution equation near the AdS boundary to satisfy the constraint equations. As a result, we obtain $V_{,v}|_{u=v} = 2Z_{,u}|_{u=v}$. Solving the boundary equation, we can determine boundary value of V at each time step.

When the pole is contained in the numerical domain, boundary conditions at the pole are necessary and the pole is fixed at $u = v + \pi/2$. Since the pole is located at $\Phi = \pi/2$, one boundary condition is given by $(Z\Psi)|_{u=v+\pi/2} = \pi/2$. The others are obtained from regularities of the evolution equations at the pole as $V_{,u} = V_{,v}$, $Z_{,u} = Z_{,v}$ and $a_{x,u} = a_{x,v}$. They are Neumann boundary conditions at the pole.

3.4 Initial data

Finally, we explain initial data for our calculations. Before turning on the electric field $V < 0$, the brane is static there. In (u, v)-coordinates, the static solution is written as

$$\begin{aligned} &V(u,v) = m^{-1}[\phi(u) + \phi(v) - \sin(\phi(u) - \phi(v))] + V_{\rm ini} \ , \quad a_x(u,v) = 0 \ , \\ &Z(u,v) = m^{-1}\sin(\phi(u) - \phi(v)) \ , \quad \Psi(u,v) = \frac{m(\phi(u) - \phi(v))}{\sin(\phi(u) - \phi(v))} \ , \end{aligned} \tag{3.20}$$

where ϕ is a free function corresponding to the residual coordinate freedom on the initial surface, and $V_{\rm ini}$ is an integration constant. At an initial surface $v = 0$, we set

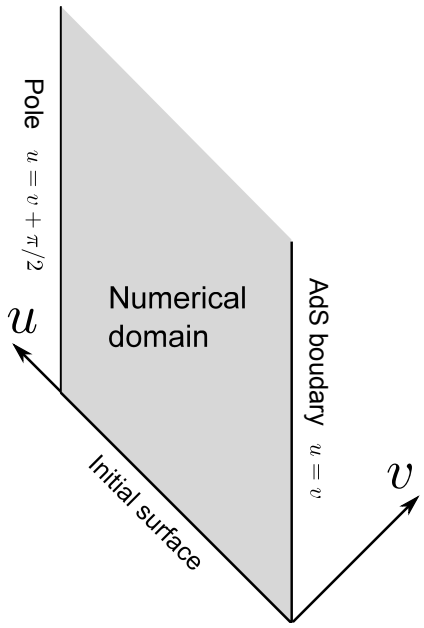

Figure 5: Numerical domain on the worldvolume of the D7-brane. The AdS boundary and the pole are fixed at $u = v$ and $u = v + \pi/2$, respectively.

initial data to be the exact solution of the static embedding in pure AdS as

$$\begin{aligned} &V(u,0) = m^{-1}(\phi(u) - \sin\phi(u)) + V_{\rm ini} \ , \quad Z(u,0) = m^{-1}\sin\phi(u) \ , \\ &\Psi(u,0) = \frac{m\phi(u)}{\sin\phi(u)} \ , \quad a_x(u,0) = 0 \ . \end{aligned} \tag{3.21}$$

We set $\phi(0) = 0$, and then $V(0,0) = V_{\rm ini} < 0$ is the initial time at the AdS boundary. At the first stage of the time evolution, when the numerical domain contains the pole, we can solve the evolution equations under choosing the free function as $\phi(u) = u$ simply. However, if there is a region which causes strong redshift on the brane such as vicinity of the event horizon, the numerical calculations will break down. To continue the numerical calculation, we pause the numerical calculation slightly before the breakdown, $v = v_{\rm int}$. We refer to the surface $v = v_{\rm int}$ as intermediate surface. We define functions at the intermediate surface as $\boldsymbol{f}_{\rm int}(u) \equiv \boldsymbol{f}(u, v_{\rm int})$ where $\boldsymbol{f} \equiv (V, Z, \Psi, a_x)$. We consider the coordinate transformation $u = \phi(\bar{u})$. Then, the v-coordinate is also transformed as $v = \phi(\bar{v})$ to locate the AdS boundary at $\bar{u} = \bar{v}$. Using $\boldsymbol{f}_{\rm int}(\phi(\bar{u}))$ as the initial data, we restart the numerical calculation from the intermediate surface, $\bar{v} = \bar{v}_{\rm int}$. We choose this free function ϕ so that V and $\bar{v}$ are synchronized up to a constant at the AdS boundary, i.e., $V|_{u=v} = \bar{v} + V_0$. For detail of numerical calculation, see [11].

4. Thermalization and deconfinement in dynamical systems

In this section, we attempt to give quantitative definitions of thermalization and deconfinement of mesons for dynamical systems in gravity side. In the boundary theory, "thermalization" means that the distribution function has settled down in thermal one; "deconfinement" means meson excitations become unstable and dissipate into the background plasma. Although both of them will occur at the same point if the systems are in equilibrium or steady state, these are physically different notions and may occur at different times in general time-dependent situations. Indeed, in the dynamical situation currently discussed, we will see that the system might not be thermalized but mesons might be deconfined. Therefore, it is important to explore means of discrimination between thermalization and dissociation in gravity.

From viewpoint of gravity, in static or stationary cases both of thermalization and deconfinement are, also, characterized by a same condition: the existence of the event horizon on the D-brane effective metric. The existence of the event horizon (precisely speaking, the Killing horizon) leads to thermal spectrum of the Hawking radiation and dissipation of excitations on the brane, which respectively correspond to thermalization and deconfinement. On the other hand, in time-dependent cases, it seems to be ambiguous how one should determine thermalization time even if event horizons will form.

Of course, black holes and event horizons can be formally defined without any ambiguities even though systems are dynamical. However, by definition, the event horizon cannot be determined unless global spacetime evolutions have been known. Temporal observers (or classical fields obeying the equations of motion) cannot know when the event horizon has formed or whether they have been inside the black hole, in principle. Alternatively, let us consider the apparent horizon instead of the event horizon. The apparent horizon can be an useful estimator to find the event horizon in dynamical spacetimes. In general cases, actually under appropriate energy conditions, apparent horizons will form inside event horizons. It means that formation of the apparent horizon does not affect physics outside the black hole. It is true that metrics irrelevant to the Einstein equations, such as an effective metric of the brane, need not satisfy physical energy conditions. (Indeed, in the current case the apparent horizon on the effective metric can form outside the event horizon.) Nevertheless, if we want to discuss black hole formation in the bulk, which correspond to thermalization of gluon plasma, the above problem is inevitable and the apparent horizon seems to have trouble with causality. Hence, appearance of the apparent horizon seems to be not so universal definition for general thermalization in the boundary theory.

In this paper, to make clear the difference between thermalization and deconfinement in the gauge/gravity duality, we will introduce the redshift factor and the

Hawking temperature for non-stationary spacetime, which are related with the retarded time. Since these quantities can be determined by the causal past of temporal observers at the AdS boundary, they give us not only practical but also physical manner to characterize horizon formations.

4.1 Definition of deconfinement

In the static case, deconfinement or confinement phases is distinguished by seeing whether there is an event horizon in the effective metric on the brane or not. However, such a naive definition cannot be used in dynamical cases such as a phase transition from confinement to deconfinement phases. Since the AdS boundary is not in the causal future of the event horizon, boundary observers cannot know "when" the event horizon is formed. To determine when the system is deconfined, we focus on the redshift factor instead of the event horizon and give a practical definition of the deconfinement time.

We consider linear perturbations of the dynamically evolving D7-brane, which correspond to meson excitations. In case of sufficiently weak electric field ($E \ll m^2$) and slow time dependence ($\Delta V \gg m^{-1}$), the linear perturbations are coming and going between AdS boundary and the pole $\Phi = \pi/2$ of the brane, namely superpositions of the normal modes with a discrete spectrum. On the other hand, in case of strong electric field ($E \gtrsim m^2$) or rapid time dependence ($\Delta V \lesssim m^{-1}$), the brane is strongly bended and there can be a region which causes strong redshift on the brane. Strong redshift means that the linear perturbations propagating for the AdS boundary are trapped and spread out in the region and can not come back to the boundary for an extremely long time. Then, boundary observers feel that the meson has dissipated into the background plasma. Thus, we can identify the existence of strong redshift on the brane with the deconfinement of mesons. This definition is nothing but practical and physical notion of black holes for temporal observers rather than formal and mathematical one. As we mentioned, temporal observers can never know truly existence of black holes and event horizons in principle. They will only observe strong redshift.

Now, we define the *redshift factor* which measures strength of the redshift as follows. We introduce a time-like vector field on the brane as $\xi = \partial_V$, where we use coordinates (V, z) defined by $V = V(u, v)$ and $z = Z(u, v)$. In term of (u, v)-coordinates, ξ is written as $\xi = J^{-1}(Z_{,v}\partial_u - Z_{,u}\partial_v)$, where J is the Jacobian: $J = V_{,u}Z_{,v} - V_{,v}Z_{,u}$. The coordinate V becomes ordinary time coordinate in the boundary metric: $ds^2 = -dV^2 + d\vec{x}_3^2$. In addition, ξ is a (locally) Killing vector in the brane effective metric before the electric field quench $V < 0$. (See Eq. (2.11).) Therefore, ξ gives us a natural time in both the boundary and initial stationary regions, while it does not has any specific meaning but one among time-like vectors in intermediate regions.

A tangent vector of out-going null geodesic on the effective metric, which is a null ray described by $u = \text{const.}$, is given by

$$k = \frac{d}{ds} = -\frac{C(u)}{\gamma_{uv}(u, v(s))}\partial_v, \tag{4.1}$$

where $C(u)$ is an integration constant associated with each null ray. Note that k is the eight-momentum of the out-going null ray, since this vector is affine parameterized in terms of s. The energy of the light ray for observers whose natural time is represented by ξ becomes

$$\omega(v) \equiv -\gamma_{ab}k^a\xi^a = \frac{C(u)Z_{,v}(u, v)}{J(u, v)}. \tag{4.2}$$

At an initial time $v = v_0$ and the AdS boundary $v = u$, the energy of the light ray becomes

$$\omega(v_0) = \frac{mC(u)}{\Phi_{,u}(u, v_0)} \ , \quad \omega(u) = \frac{C(u)}{V_{,v}(u, u)} \ . \tag{4.3}$$

We have used for the former equation the static solution (3.20) at $v = v_0$ and for the latter equation the boundary conditions at the AdS boundary: $V_{,u} = 0$, $V_{,v} = 2Z_{,u}$, and $Z_{,u} = -Z_{,v}$. As a result, the redshift factor, which is the ratio between the energy observed on the boundary and the initial energy, is given by[6]

$$R(u) \equiv \frac{\omega(v_0)}{\omega(u)} = \frac{m}{2}\frac{V_{,v}(u, u)}{\Phi_{,u}(u, v_0)}. \tag{4.4}$$

For supersymmetric embedding, $Z = m^{-1}\sin\Phi$, since this energy $\omega(v)$ becomes the Killing energy with respect to the Killing vector ∂_V and it should be conserved, we have $R = 1$. Also, the initial time v_0 can be taken arbitrary as far as stationary regions. Roughly speaking, this quantity represents how the energy of the light ray emitted in the infinite past is red-shifted when the ray has arrived at the boundary. If $R(u)$ is infinity, such null ray cannot reach the boundary. When an event horizon will be formed, $R(u)$ will tend to diverse by definition.

In our calculations, if this redshift factor $R(u)$ observed at the AdS boundary is so large ($R > 100$), we shall say that the system becomes deconfinement phase.

[6] A past directed null geodesic from the AdS boundary may reach the pole before the initial surface. Then, we assume that the null geodesic is reflected at the pole and the AdS boundary. After several reflections, it reaches the initial surface eventually. Taking into account the reflections, the expression for the redshift factor is modified as

$$R(u) = \frac{m}{2}\frac{V_{,v}(u, u)}{\Phi_{,u}(u - \pi n/2, v_0)} \ ,$$

where we have used the coordinates defined in section 3.3. The integer n is chosen so that $0 \leq u - \pi n/2 \leq \pi/2$ is satisfied.

4.2 Definition of thermalization

Because of the same reason as the deconfinement, the formation of horizons cannot be a good definition of the thermalization in dynamical cases. Here, in order to clarify thermalization in gravity side, we use the Hawking temperature for time-dependent cases based on semi-classical arguments [40, 41]. By using the redshift factor, we can define the following quantity

$$\kappa(u) \equiv \frac{1}{V_{,v}(u,u)} \frac{d}{du} \log R(u), \tag{4.5}$$

where $V_{,v}(u,u)$ denotes the normalization in terms of the boundary time. This describes "peeling property" of out-going null geodesics, which corresponds to "surface gravity" for the past horizon when initial state is finite temperature.[7] One can find that, if evolutions of $\kappa(u)$ are sufficiently slow, spectrum of the Hawking radiation becomes approximately thermal with the temperature determined by $\kappa(u)$. When the system settles down in stationary, this temperature eventually agrees with the ordinary Hawking temperature associated with the Killing horizon, of course. Therefore, we shall define thermalization by saying that $\kappa(u)$ has been close to the final temperature.

Intuitively, since the redshift factor represents the relation between the natural times, the relation of creation-annihilation operators between initial state and final one is determined by $\kappa(u)$. In particular, situations of the current model are quite similar to considering quantum fluctuations in the so-called moving mirror model. This is because, for the fluctuations on the brane, the pole can be regard as a mirror (in fact, we have imposed the Neumann boundary condition there) and dynamics of the brane will cause this mirror to move effectively. Thus, this surface gravity $\kappa(u)$ defined above is just the quantity which characterizes particle creations caused by the moving boundary.

We note that $R(u)$ and $\kappa(u)$ are closely related but different quantities. If a system settles down in the final steady state with the horizon, $R(u)$ becomes exponentially very large and then $\kappa(u)$ becomes a constant value. This implies that the mesons has been dissociated and the system has been thermalized in the boundary theory. However, even if $R(u)$ becomes so large that the horizon (or naked singularities) would be formed, $\kappa(u)$ does not always settle down. Such cases can be interpreted as the phase in which mesons are dissociated but non-thermalized.

In our calculations, we shall adopt $|\kappa - \kappa_f|/\kappa_f < 0.01$ as criteria for thermalization, where κ_f is the final value of the surface gravity.

[7] If the initial state is at a finite temperature, it means that the past horizon should exist in gravity side. In such cases we should define the redshift factor by using the Kruskal time, which is natural initial time on the past horizon, instead of the Killing time.

5. Results for supercritical electric fields

In our setup, time evolutions of the D-brane are characterized by two model parameters $(E_f/m^2, m\Delta V)$, which are a final value and a rise time of the homogeneous electric field. For the static case, there is a critical value of the electric field $E_{\rm crit} = 0.5754m^2$ below which only the Minkowski embeddings exist as shown in section 2. We study the time evolutions of the brane dividing the parameter space into two regions: supercritical electric field $E_f > E_{\rm crit}$ and subcritical electric field $E_f < E_{\rm crit}$. We will show numerical results for supercritical electric fields in this section and for subcritical ones in the next section. In appendix D, we estimate error in our numerical calculations.

5.1 Brane motion and boundary observable

Figure 6(a) shows snapshots of the time evolution of the D7-brane embeddings for $E_f/m^2 = 1$ and $m\Delta V = 0.5$. As vertical and horizontal axes, we have taken Cartesian-like coordinates, $w = z^{-1}\sin\phi$ and $\rho = z^{-1}\cos\phi$. The dashed curve shows the effective event horizon for the static embeddings with the parameter $E/m^2 = 1$. At the late time, the brane configuration tends to be static and eventually coincides with the static black hole embedding shown in section 2.

From the numerical solution, we can find the event and apparent horizons on the effective metric (3.7). Since we are using double-null coordinates, the condition for the apparent horizon is simply written as

$$\partial_v \left[\frac{\cos^3\Phi}{Z^3} \left(\frac{h_{uv} + Z^2 f_{ux} f_{vx}}{h_{uv} - Z^2 f_{ux} f_{vx}} \right)^{1/2} \right] = 0 \ . \tag{5.1}$$

Solving the above equation, we obtain the location of the apparent horizon $u = u_{\rm AH}(v)$. The event horizon is defined by the boundary of the causal past of the AdS boundary. We denote the event horizon as $u = u_{\rm EH}$. (The $u_{\rm EH}$ is a constant since the event horizon is a null surface.) In Fig. 6(b), we show the locus of event and apparent horizons in (t, z)-coordinates: $(t(u_{\rm EH}, v), z(u_{\rm EH}, v))$ and $(t(u_{\rm AH}(v), v), z(u_{\rm AH}(v), v))$.[8] Here, t is the ordinary time coordinate: $t \equiv V + z$. Note that these effective horizons on the brane worldvolume are different from bulk ones. (Actually, there is no black hole horizon in the bulk since it is pure AdS now.) Especially, the effective event horizon is time like in the view of the bulk metric and can be seen from the AdS boundary through the bulk null geodesic. The event and apparent horizons intersect each other and the apparent horizon is outside the event horizon in several places. This implies that the effective metric violates the null energy condition. (Since

[8]Strictly speaking, the location of the event horizon can not be determined unless whole time evolution has been known by the infinite future on the AdS boundary. Since, however, we can solve time evolutions only during a finite time by practical numerical calculations, we have approximately estimated the location of this event horizon by using the latest time of the numerical calculation.

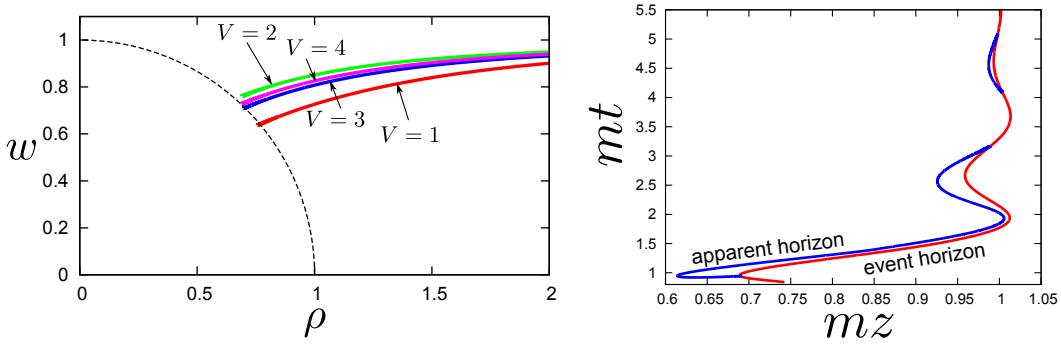

(a) snapshots of the brane

(b) effective horizons

Figure 6: (a)Snapshots of embeddings of the D7-brane in (w, ρ)-plane. We take the unit of $m = 1$ and set parameters as $E_f/m^2 = 1$ and $m\Delta V = 0.5$. For static embedding, the effective horizon is located at $w^2 + \rho^2 = E = 1$, which is shown by a dashed curve in this figure. (b)Event and apparent horizons. The vertical axis is the ordinary time coordinate in the bulk: $t \equiv V + z$.

the effective metric does not obey the Einstein equations, this condition has just a geometrical meaning.) Therefore, theorems in general relativity based on the null energy condition, such as Hawking's area theorem, do not hold for brane dynamics.

Now, we turn to quantities on the boundary theory. Figure 7 shows quark condensate c and electric current j as functions of boundary time V. As typical examples for supercritical electric fields, we show our numerical results for $(E_f/m^2, m\Delta V) = (1, 1), (1, 0.5), (2, 0.5)$, and $(2, 1)$. Although the quark condensate and the electric current oscillate at the first stage of the time evolutions, they approach constant values at the late time.[9] This means that the fluctuations on the brane have dissipated in the effective event horizon. For the static embeddings, the quark condensate and the electric current are given by $(c/m^3, j/m^3) = (-0.297, 0.331)$ and $(-0.751, 1.81)$ for $E/m^2 = 1$ and 2, respectively. We can confirm that these values coincide with the asymptotic values of c and j for the dynamical cases.

5.2 Thermalization and deconfinement time

In this subsection, we study thermalization and deconfinement based on the definitions introduced in section 4. In Fig. 8, we show the redshift factor R and the surface gravity κ as the boundary time V for several parameters $(E_f/m^2, m\Delta V) = (1, 1), (1, 0.5), (2, 0.5)$, and $(2, 1)$. In section 4, we have defined a criterion of the deconfinement as $R = 100$ which is shown by the horizontal line in Fig. 8(a). Since the redshift factors increase exponentially at the late time, they exceed the criterion and the systems change to deconfinement phases. On the other hand, we have defined the thermalization by $|\kappa - \kappa_f|/\kappa_f < 0.01$ where κ_f is the final value of the surface

[9]It would be interesting to compare our maximum oscillation with the universal scaling found in [52] (see also [21]). However, our case is not conformal as we have the mass scale m.

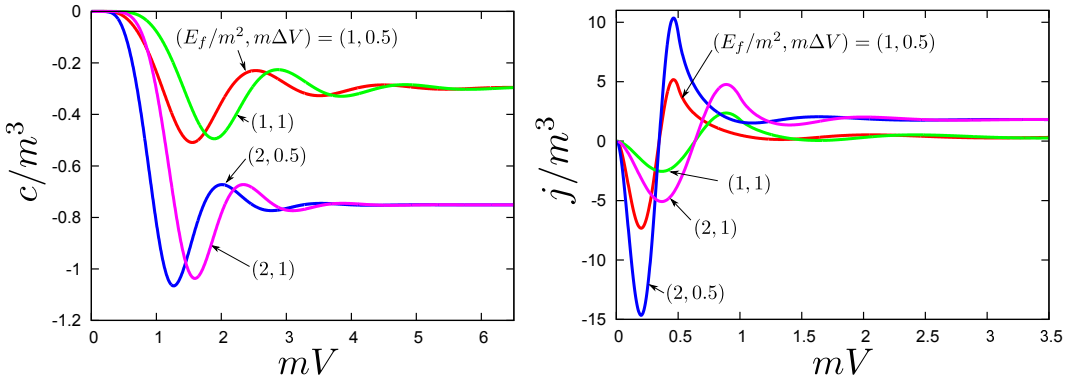

(a) quark condensate (b) electric current

Figure 7: Time dependence of quark condensate c and electric current j for $(E_f/m^2, m\Delta V) = (1,1), (1,0.5), (2,0.5)$, and $(2,1)$. Note that while the electric field is time-dependent (namely $0 < V < \Delta V$), the obtained value of j has a slight uncertainty. This is because unhealthy behavior of the equations of motion seems to affect numerical error.

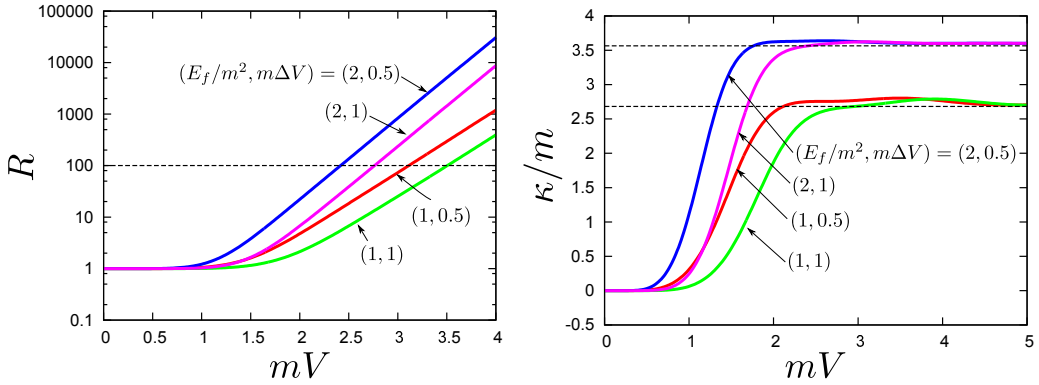

(a) redshift factor (b) surface gravity

Figure 8: Time dependence of redshift factor R and surface gravity κ for $(E_f/m^2, m\Delta V) = (1,1), (1,0.5), (2,0.5)$, and $(2,1)$.

gravity.[10] The criteria for $E_f/m^2 = 1, 2$ are shown by horizontal lines in Fig. 8(b). We see that the systems have been thermalized at the late time.

In Fig. 9(a), we show the thermalization time $t_{\rm th}$ as a function of final value of the electric field E_f. At the critical value of the electric field $E_f = 0.5754m^2 \equiv E_{\rm crit}$, the thermalization time appears to diverge. This is natural behavior because, for $E_f < E_{\rm crit}$, there are no static black hole embeddings and the system has never been thermalized. In contrast, the thermalization time becomes small as E_f increases. This is because the brane fluctuations are damped by $\sim e^{-\kappa V}$ as general features for quasi-normal modes and, thus, we can estimate the thermalization time as $t_{\rm th} \sim$

[10] We evaluated κ_f from static embeddings.

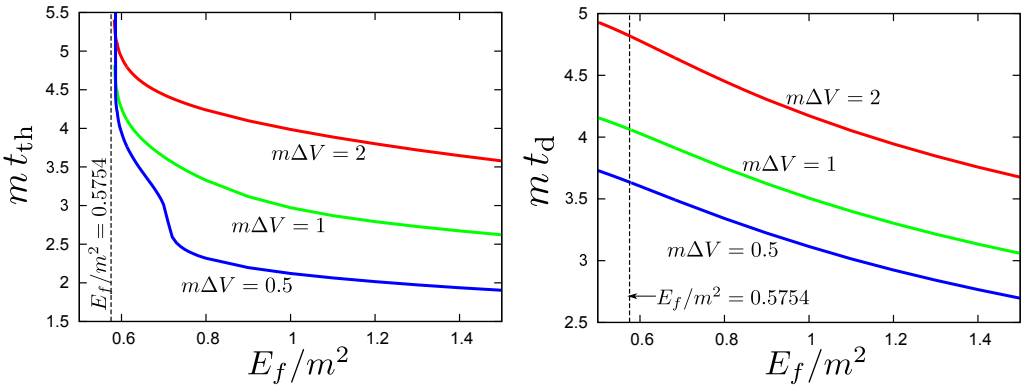

(a) thermalization time (b) deconfinement time

Figure 9: Thermalization and deconfinement time as functions of E_f.

$1/\kappa \sim 1/\sqrt{E_f}$.[11] This is nothing but the Plankian thermalization time pointed out in Ref. [26].

In Fig. 9(b), we show the deconfinement time $t_{\rm d}$ as a function of E_f. The $t_{\rm d}$ is finite at the critical electric field $E_f = E_{\rm crit}$. Furthermore, even for $E < E_{\rm crit}$, it is conceivable that the system becomes deconfinement phase if the system is dynamical. We will discuss the deconfinement below the critical electric field in detail in the next section.

6. Results for subcritical electric fields

6.1 Quark condensate and electric current

In this section, we show numerical results for subcritical electric fields. First, we study the quark condensate and electric current for $E_f/m^2 = 0.01$ and $m\Delta V = 1.0$, in which the electric field is sufficiently weak. Figure 10 shows time dependence of the electric current j and the quark condensate c. Figures (a) and (b) show an early stage of the time evolution $0 \leq mV \leq 10$, while (c) and (d) show the time evolution over a long time $0 \leq mV \leq 620$.

In the static case, only the Minkowski embedding exists and the electric current is exactly zero for the electric field $E/m^2 = 0.01$ as in Fig. 4(b). However, in dynamical cases, just after turning on the electric field ($V \geq 0$), the electric current starts to oscillate with a finite amplitude as well as the quark condensate. This corresponds to the oscillation of the bound state of quarks in the boundary theory, that is polarization current. In our setup, this oscillation does not dissipate since the energy of the D-brane is conserved within the probe approximation $N_f \ll N_c$. This is nothing but a non-linear counterpart of the normal mode in linear perturbations.

[11] Below Eq. (2.17), we showed that the surface gravity is given by $\kappa \simeq (6E)^{1/2}$ for $E \to \infty$.

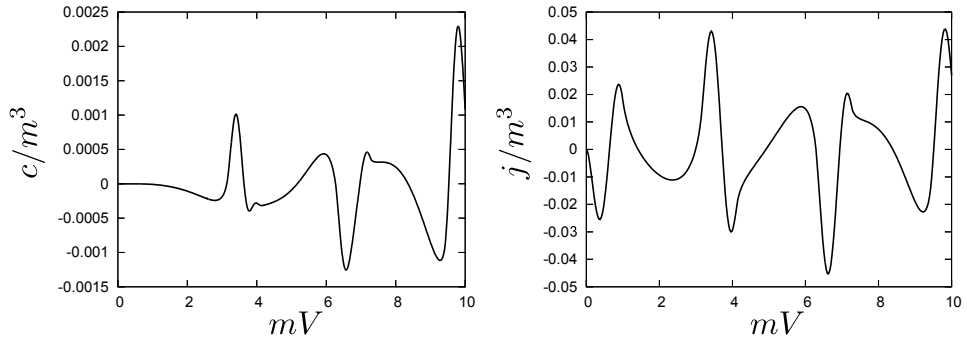

(a) quark condensate for $0 \leq V \leq 10$ (b) electric current for $0 \leq V \leq 10$

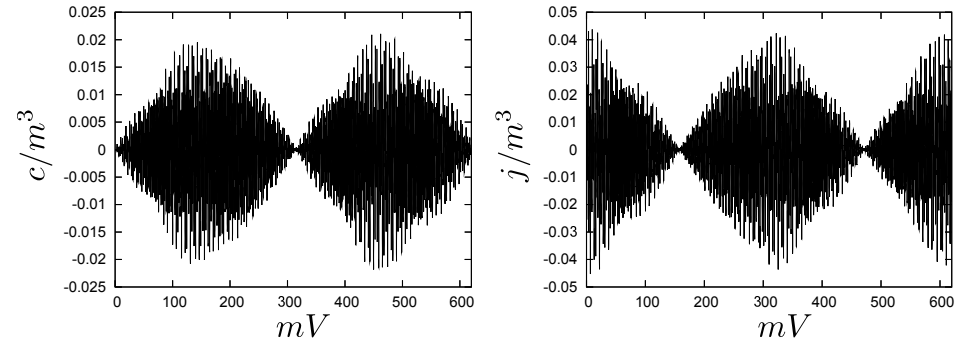

(c) quark condensate for $0 \leq V \leq 620$ (d) electric current for $0 \leq V \leq 620$

Figure 10: Time dependence of quark condensate c and electric current j for $E_f/m^2 = 0.01$ and $m\Delta V = 1$.

The time evolution over a long period shown in Figs. 10(c) and (d) reveals that there are beats with the oscillations for both of the quark condensate and the electric current. The beat represents the energy exchange between the brane fluctuation $\Phi(V, Z)$ and the gauge potential on the brane $a_x(V, Z)$ because the phase of each beat is opposite. In the case of zero electric field, they are regarded as coherent oscillations of scalar and vector mesons,[12] whose mass spectra degenerate [42]. Therefore, the beat represents the mixing of scalar and vector mesons caused by the presence of the external electric field. Figure 11 shows the beat frequency $\omega_{\rm beat}$, which is defined based on period of each node of the envelope, for several values of the electric field E_f. By linear fitting we can find $\omega_{\rm beat} \simeq 2.0 E_f/m$. This implies the mass spectra for the scalar and vector mesons split because of the Stark effect and then it results in the mass difference $\delta M \simeq \omega_{\rm beat}$. In appendix C, we evaluate the shifts of spectra for a weak electric field and find $\omega_{\rm beat} = 2E_f/m$, analytically. This is consistent with our numerical results and the perturbative calculation is so reasonable at least for $E/m^2 \lesssim 0.02$.

[12]From Eq. (3.1), we find $\partial^\mu A_\mu = 0$ ($\mu = V, x_1, x_2, x_3$) for $a_u = a_v = 0$. Thus, the oscillation of a_x represents the excitation of a vector meson.

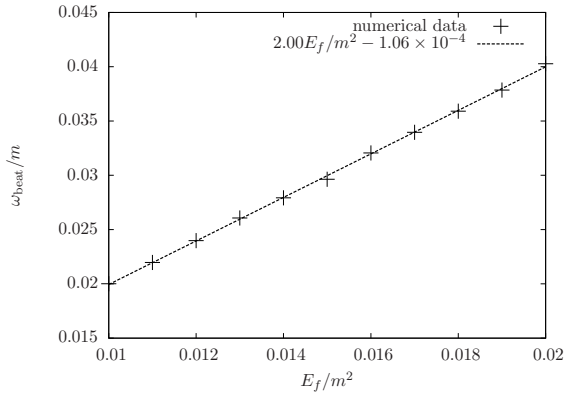

Figure 11: Relation between the beat frequency $\omega_{\rm beat}$ and final value of the electric field E_f. Dashed line is obtained by linear fitting as $\omega_{\rm beat}/m = 2.00E_f/m^2 - 1.06 \times 10^{-4}$.

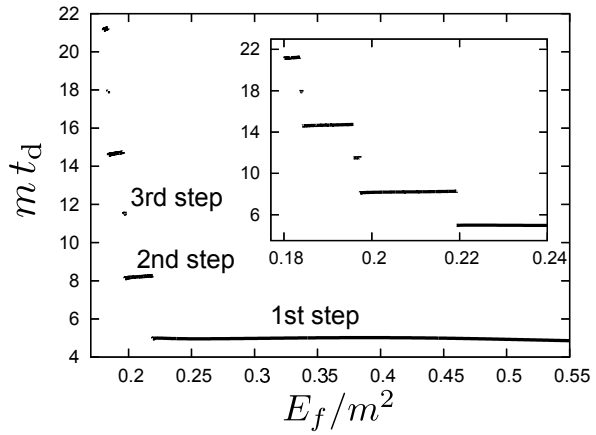

Figure 12: Deconfinement time $t_{\rm d}$ against electric field E_f for $m\Delta V = 2$. It is a discrete function and almost constant at each step. From the bottom, we refer to each step as 1st step, 2nd step, and so on.

6.2 Deconfinement below the critical electric field

Now, we focus on moderate subcritical electric fields. In such cases we can observe fascinating phenomena characteristic of dynamical situations. As we mentioned, for $E_f < E_{\rm crit}$, the system will never be thermalized since no static black hole embedding exists as the final state. In fact, in Fig. 9(a), we have seen that the thermalization time appears to diverge at the critical electric field. However, this does not mean that deconfinement is impossible below the critical electric field.

In Fig. 12, we plot the deconfinement time $t_{\rm d}$ as a function of E_f for $m\Delta V = 2$ and $E/m^2 < 0.55$. We can find that the $t_{\rm d}$ is a discrete function of E_f and almost constant at each step, which is referred to as 1st step, 2nd step, and so on. To understand this curious behavior in the deconfinement time in terms of the brane

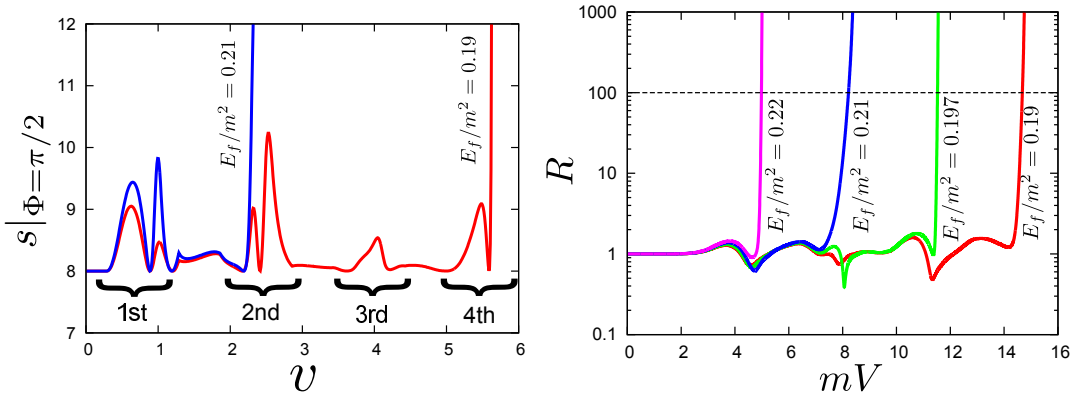

(a) a scalar quantity s at the pole (b) redshift factor

Figure 13: (a)Time dependence of the scalar quantity s at the pole for $E_f/m^2 = 0.21, 0.19$ and $m\Delta V = 2$. They are on 2nd and 4th steps, respectively. (b)Time dependence of the redshift factor R for $E_f/m^2 = 0.22, 0.21, 0.197, 0.19$ and $m\Delta V = 2$. They are on 1st, 2nd, 3rd, and 4th steps, respectively.

dynamics, we define a scalar quantity on the brane worldvolume, $s \equiv \gamma^{ab}h_{ab} = 4(\gamma_{uv} + h_{uv})/\gamma_{uv}$, and investigate the time evolution of s evaluated at the pole $\Phi = \pi/2$. Note that, since the stress tensor of the brane is proportional to γ^{ab}, we can interpret $s|_{\Phi=\pi/2}$ as a rough indication of the energy density at the pole.

In Fig. 13, we plot $s|_{\Phi=\pi/2}$ as a function of the brane coordinate v for $E_f/m^2 = 0.21$, 0.19 and $m\Delta V = 2$. These correspond to 2nd and 4th steps in Fig. 12. We can see that pulses are localized in several time intervals which are shown by 1st, 2nd, 3rd and 4th in the figure. This is because the fluctuation on the brane caused by turning on the electric field is reflected at both sides of the AdS boundary and the pole. It propagates between these boundaries several times. For $E_f/m^2 = 0.21$, when the wave packet comes to the pole for the second time, the scalar quantity seems to be diverging. On the other hand, for $E_f/m^2 = 0.19$, it seems to be diverging when the wave packet comes to the pole for the fourth time. The divergence of the scalar quantity implies the appearance of a singularity on the brane. Figure 14 gives a schematic picture of this behavior. This behavior is similar to the weakly turbulent instability of AdS spacetime: AdS is non-linearly unstable under arbitrarily small perturbations [53]. Detailed analysis of the "weakly turbulent instability of D-brane" and its implication for the field theory will be discussed elsewhere.

We can expect that, when the s becomes large, the brane is strongly bended and a region which causes strong redshift will appear on the brane. Actually, in Fig. 13, we find that the redshift factor diverges at the same time as the divergence of s in retarded time.[13] It turns out that the divergence of the redshift factor R is extremely rapid within a finite boundary time rather than the exponential divergence

[13]When the scalar quantity $s|_{\Phi=\pi/2}$ diverges at $(u, v) = (u_0, u_0 - \pi/2)$, the retarded time is defined by $V(u_0, u_0)$ at the AdS boundary.

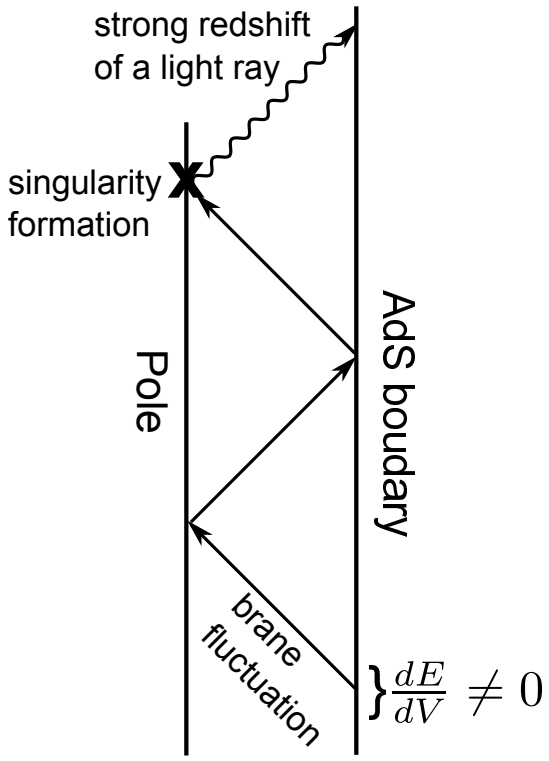

Figure 14: A Penrose diagram of the brane worldvolume. A brane fluctuation is injected from the AdS boundary for $0 \leq V \leq \Delta V$ since the electric field is time dependent there. It is reflected at the pole and the AdS boundary several times. Eventually, it collapses at the pole and appears to form a naked singularity. (The number of bounces depends on the parameters, E_f and ΔV.) A light ray going through near the singularity is strongly redshifted.

in the case where the system can be thermalized. This implies that the singularity is naked and not hidden by an event horizon. Since almost only the number of bounces determines the divergence of the redshift factor, the deconfinement time is discrete and almost constant at each step. It takes $v = \pi/2$ for one round trip in the worldvolume coordinate. If static embeddings with zero electric field, we have $V(v, v) = 2v/m$. Thus, the difference of the deconfinement time for each step can be roughly estimated as $\Delta t_{\rm d} \simeq \pi/m$.

The number of bounces needed for the divergence of s depends on parameters E_f and ΔV. We examine its dependence on two parameters $(E_f/m^2, m\Delta V)$ and summarize the result in Fig. 15. Each curve represents the boundary of the number of bounces needed for the formation of the naked singularity. For example, above the red curve, the singularity is formed when the wave packet reaches the pole at the first time. Between the red and green curves, it is formed at the second time. (They correspond to the 1st and 2nd steps in Fig. 12.) Note that below the light blue curve we can successively find and draw many curves. Practically, we can only perform

numerical calculations over a limited period of time and with a limited resolution. It is not so clear whether the region below the light blue curve is filled with an infinite number of the curves or there is a threshold below which the instability does not occur.[14] (For the parameters shown in Fig. 10 of the previous subsection, we have not observed any evidence that a singularity forms at least within $0 \leq mV \leq 620$.) However, since areas surrounded by those curves become too narrow to distinguish each one, we have omitted drawing them in the figure. As $m\Delta V$ becomes larger, the curves will approach asymptotically to the critical line $E_{\rm crit}/m^2 = 0.5754$ which is the critical electric field in the static case. This is because large ΔV means the electric field is introduced adiabatically and then the deconfinement transition may occur near the static critical value. Note that for large ΔV dynamics of the brane will begin to depend on the profile of $E(V)$. Although precise orbits of the curves shown in the figure might not be universal, qualitative behavior should not change.

Using the observables in boundary theory, vertical and horizontal axis of Fig. 15 are written as

$$\frac{E_f}{m^2} = \sqrt{\frac{\lambda}{2\pi^2}}\frac{\mathcal{E}}{m_q^2} = 8\sqrt{\frac{2\pi^2}{\lambda}}\frac{\mathcal{E}}{m_{\rm gap}^2} \ , \qquad m\Delta V = \sqrt{\frac{2\pi^2}{\lambda}} m_q \Delta V = \frac{\sqrt{2}}{4} m_{\rm gap}\Delta V \ , \quad (6.1)$$

where $m_{\rm gap} \equiv 4\pi m_q \lambda^{-1/2}$ is mass gap in $\mathcal{N} = 2$ SQCD [42]. In according to the RHIC experiment, we set parameters as $\mathcal{E}/m_{\rm gap}^2 \sim 0.02$ and $m_{\rm gap}\Delta V \sim 0.4$ [3]. Then, we obtain $E_f/m^2 \sim 0.6/\sqrt{\lambda}$ and $m\Delta V \sim 0.1$. From Fig. 15, the system can be in deconfinement phase at least for $E_f/m^2 \gtrsim 0.01$. Therefore, our result indicates that, if the 't Hooft coupling satisfies $\lambda \lesssim 10^3$, the system can be in deconfined phase even though it is not thermalized in RHIC experiment.

Now, we set parameters as $E_f/m^2 = 0.3, 0.5$ and $m\Delta V = 1$. For these parameters, the system will be deconfined although the electric field is below the critical value. Figure 16 shows time dependence of the electric current j and quark condensate c. They oscillate and does not converge. As shown before, the scalar quantity s tends to be diverging within a finite time, while, in c and j, we do not find any singular behavior. (The right ends of the curves in Fig. 16 correspond to the time of divergence of s in retarded time.) This is, presumably, because the singularity near the pole will form suddenly (the divergence of the redshift factor is extremely rapid). As a result, these observables in the boundary theory does not respond and remain finite. However, the singularity, in which we have to take into account the various effects beyond the current probe approximation, is naked, namely visible from the AdS boundary.[15] We can expect to observe interesting phenomena such as quantum effect on the brane, backreaction to the bulk spacetime, and so on.

[14] If one takes into account backreactions beyond the probe approximation, the energy of the oscillations on the brane will dissipate via emitting closed strings over a long period. In such case, the instability after a huge number of the bounces may be physically irrelevant.

[15] The fast oscillation of the brane in the target spacetime is T-dual to a D-brane with electric field

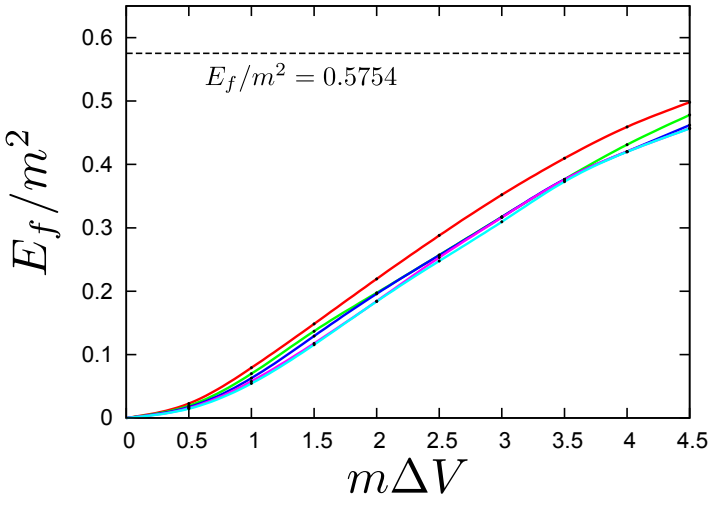

Figure 15: Parameter space of time-dependant solutions of D7-brane. These curves represent the boundaries of the number of bounces needed for the formation of naked singularity. Black points are our numerical data. We have interpolated them by spline curves passing through the origin. $E_f/m^2 = 0.5754$ (dashed line) is the critical electric field in the static case.

For example, in order to estimate quantum effect on the brane, let us consider minimally coupled massless field on the (1+1)-dimensional part of the brane effective metric. We introduce two kinds of null coordinates u and U, which are retarded times to define positive frequency modes in a final state and an initial state, respectively. Then, assuming the initial state does not have any out-going flux, the expectation value of the stress tensor of the massless field is given by

$$\langle T_{uu} \rangle \sim -\frac{1}{24\pi}\{U, u\} = \frac{1}{48\pi}\left[\left(\frac{U''}{U'}\right)^2 - 2\left(\frac{U''}{U'}\right)'\right], \tag{6.2}$$

where $\{U, u\}$ is the Schwarzian derivative and the prime denotes u-derivative. (See Ref. [54], for example.) Recalling the fact that the redshift factor is relation between the initial time and the final time associated with out-going null geodesics, one can find $R(u) = 1/U'(u)$ and $\kappa(u) = -U''(u)/U'(u)$. Thus, we have out-going flux of particle creation as $\langle T_{uu} \rangle \sim (\kappa^2 + 2\kappa')/(48\pi)$. When the effective horizon is formed ($\kappa(u) \sim$ const.), this out-going flux leads to thermal flux of the final steady state. On the other hand, when the naked singularity emerges, it may blow up because the divergence of $R(u)$ is extremely rapid.

on it. The open string metric on the D-brane with large electric field shows a peculiar property (emergent Carrollian metric) where the light cone collapses [51], and it would be related to our deconfinement.

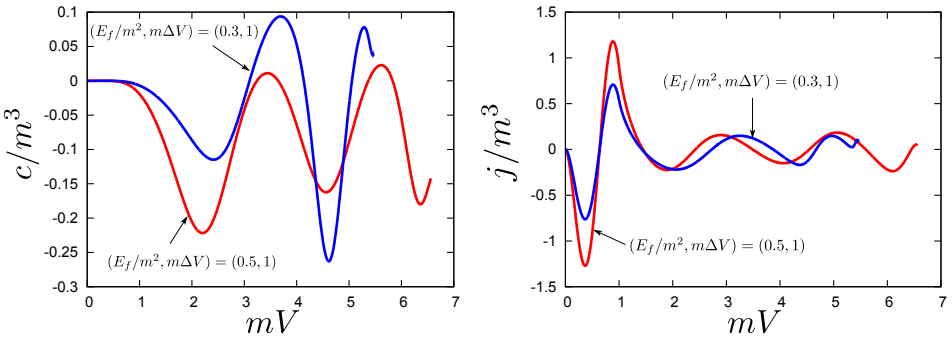

(a) quark condensate (b) electric current

Figure 16: Time dependence of quark condensate and electric current j for $(E_f/m^2, m\Delta V) = (0.5, 1)$ and $(0.3, 1)$.

7. Conclusion and discussions

In this paper, we analyzed response of the strongly coupled gauge theory against an electric field quench, by using the AdS/CFT correspondence. The system is $\mathcal{N} = 2$ supersymmetric QCD with $\mathcal{N} = 4$ super Yang-Mills as a gluon sector, and has a confining spectrum for the meson sector (while the gluon sector is always deconfined). We turn on the electric field in a time-dependent manner, and find that the system develops to a deconfinement phase of mesons.

We have studied time-dependent behavior of various observables such as electric current carried by the quarks and the quark condensate. We have defined the thermalization time scale and the deconfinement time in terms of the gravity dual side: the thermalization is with the Hawking temperature, and the deconfinement is with the strong redshift.

Among our findings, the most interesting is the fact that the deconfinement transition of the mesons occurs even with a small electric field once it is applied time-dependently. In the static electric field, there exists a critical value of the electric field beyond which the electric current flows and the system is deconfined. In our time-dependent quench, if the quench is made sufficiently fast, even with a final electric field which is smaller than the critical value, the system goes to a deconfinement phase — there appears a strong red shift region in the gravity dual. See section 6 for details.

In the dual gravity picture, this phenomena can be understood as the D-brane version of the weakly turbulent instability [53]: The wave packet on the D-brane is getting sharp as time increases and, eventually, collapses into the naked singularity. Accordingly, we also found a curious behavior of the deconfinement time — the time scale when a strong redshift region appears on the D7-brane. The deconfinement time takes only discrete values, see Fig. 12.

We also found that when the applied electric field is small enough, the decon-

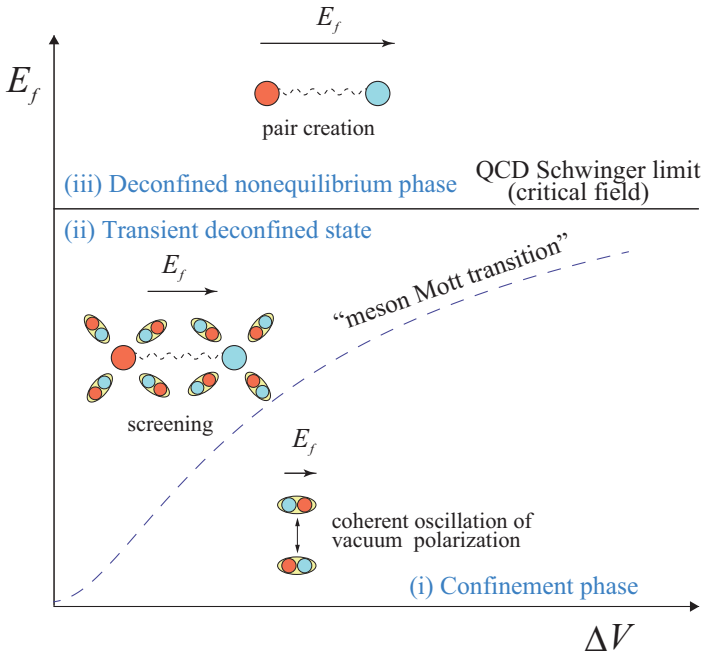

Figure 17: Schematic "dynamical phase diagram" of states realized in the present study by a static electric field E_f following an initial ramp (parametrized by the time parameter ΔV). See text for details.

finement transition does not occur within a practical time-scale , but there appears a beat frequency which dictates the energy inflow-outflow between the chiral condensate and the electric current, see Fig. 10 (c) and Fig. 10 (d). Each corresponds to the scalar fluctuation and the gauge fluctuation on the D7-brane. The beat frequency is found to be proportional to the electric field value. This fact can be well explained by the analytic formula of the mass splitting for the Stark effect.

Our findings are of course a consequence of the analyses performed in the gravity dual side, and they wait for possible interpretation in the gauge theory side. It is encouraging that even with a small electric field, if it is applied sufficiently fast, it leads to a deconfinement phase. Its implication to heavy ion collision experiment would be important.

Furthermore, the potential implication of the present study of nonequilibrium dynamics in QCD to strongly correlated electron system is suggestive. In condensed matter, nonequilibrium dynamics of correlated electrons induced by strong electric fields is being intensively studied experimentally [55–58] and theoretically [59–64]. Strong Coulomb interaction between electrons can freeze the electrons' motion leading to an insulating state known as the Mott insulator [65]. Charge excitations, called doublons and holons, are energetically forbidden in this phase. By applying very strong static [55] or pulse [56, 57] electric fields, one can break the insulating state by creation of charge excitations. If the field is not strong enough, the created

charges may be bounded by the attractive force and form excitons, i.e., pairs of plus and minus charges. Excitons do not carry direct electric current and the system is insulating. However, there is an old and interesting proposal: "When the density of the excitons exceeds a critical value, the attractive force becomes screened and the excitons become dissolved leading to a plasma of charged particles". This transition is called the exciton Mott transition (or crossover) [63, 68–70] and was recently observed experimentally [58]. The excitons in condensed matter can be related to mesons in the present system. Then, it is tempting to speculate that the formation of naked singularity explained in the previous section is an indication of the "meson Mott transition", i.e., the QCD version of the exciton Mott transition. We plot a schematic phase diagram obtained by this analogy in Fig. 17 with three regions (i), (ii), and (iii).

(i) Confinement phase with coherent oscillation When the field is weak, the system is always in the confinement phase. However, when the ramp speed is fast (small ΔV), the field induces a coherent oscillation of vacuum polarization due to meson excitation. The field during the ramp (3.18) can be considered as a pulse field with a frequency parameter $\Omega = 2\pi/\Delta V$. When Ω is comparable with the meson energy, (multi-)photon absorption process becomes possible [61, 66, 67] and leads to excitation below the critical field. We note that a similar oscillation of current was observed in a condensed matter model [60].

(ii) Transient deconfined phase ("meson Mott transition") This is the speculated "meson Mott transition" regime. When the meson amplitude becomes large, the confinement force becomes relatively weak due to screening. The quarks become liberated and deconfinement takes place in the meson (quark) sector [16]. The dashed line that separates this region with (i) corresponds to the infinite bounce limit of Fig. 15.

Since the field is below the critical field, the static solution obtained by adiabatically introducing the field ($\Delta V \to \infty$) is in the confinement phase. Thus, we expect that the plasma state realized by the meson Mott transition is transient. In the long time limit, pair annihilation of quarks dominates and the plasma disappear. Detailed time evolution in this region is still unclear and is an interesting future problem.

(iii) Deconfined nonequilibrium phase above QCD Schwinger limit When the electric field is stronger than the confining strength (= QCD Schwinger limit),

[16] There is a difference between the present situation compared to previous theories of exciton Mott transition, e.g., [63]. The latter is typically considered in a static state, i.e., finite density gas of excitons in equilibrium, while our system experience a coherent oscillation of the mesons. The coherent oscillation accelerates the deconfinement since the dynamics leads to energy dissipation and heating.

the confinement phase becomes unstable against direct pair creation of quark and antiquarks [26]. This state is a static nonequilibrium phase with finite current [23].

In summary, by studying the dynamics of supersymmetric QCD in strong electric fields, we observed many interesting, and universal nonequilibrium physics. Our finding implies similarities between possible formation mechanism of quark gluon plasma in heavy ion collision experiments to laser induced phase transitions in condensed matter, which helps us understand the physics more deeply.

Acknowledgments

We are grateful to Takahiro Tanaka for helpful discussions. K.H. would like to thank Rikkyo university for hospitality. K.H. and T.O. are supported by KAKENHI (Grant No. 23654096, 24224009, 26400350). This research was partially supported by the RIKEN iTHES project.

A. Equations of motion from the DBI action

In this appendix, we will summarize general features of the equations of motion from the DBI action.

The DBI action for Dp-brane is

$$S_{\mathrm{D}p} = \int d^{p+1}\sigma \sqrt{-\det(M_{ab})}, \tag{A.1}$$

where $M_{ab} = h_{ab} + f_{ab}$. For convenience we adopt the following abbreviated notation for describing matrices:

$$\mathbf{M} = \mathbf{h} + \mathbf{f}, \quad \mathbf{M}^{-1} = \mathbf{h}^{-1} - \mathbf{h}^{-1}\mathbf{f}\mathbf{h}^{-1} + \mathbf{h}^{-1}\mathbf{f}\mathbf{h}^{-1}\mathbf{f}\mathbf{h}^{-1} - \cdots, \tag{A.2}$$

$${}^{t}\mathbf{M} = \mathbf{h} - \mathbf{f}, \quad {}^{t}\mathbf{M}^{-1} = \mathbf{h}^{-1} + \mathbf{h}^{-1}\mathbf{f}\mathbf{h}^{-1} + \mathbf{h}^{-1}\mathbf{f}\mathbf{h}^{-1}\mathbf{f}\mathbf{h}^{-1} + \cdots, \tag{A.3}$$

where $\mathbf{h}$ is symmetric and $\mathbf{f}$ is anti-symmetric.

The symmetric part of $\mathbf{M}^{-1}$ is

$$\begin{aligned} \boldsymbol{\gamma}^{-1} =& (\mathbf{M}^{-1} + {}^{t}\mathbf{M}^{-1})/2 \\ =& \mathbf{h}^{-1} + \mathbf{h}^{-1}\mathbf{f}\mathbf{h}^{-1}\mathbf{f}\mathbf{h}^{-1} + \mathbf{h}^{-1}\mathbf{f}\mathbf{h}^{-1}\mathbf{f}\mathbf{h}^{-1}\mathbf{f}\mathbf{h}^{-1}\mathbf{f}\mathbf{h}^{-1} + \cdots \\ =& (\mathbf{I} + \mathbf{X}^2 + \mathbf{X}^4 + \cdots)\mathbf{h}^{-1}, \end{aligned} \tag{A.4}$$

where we have defined $\mathbf{X} \equiv \mathbf{h}^{-1}\mathbf{f}$. Shortly, we obtain

$$\boldsymbol{\gamma} = \mathbf{h}(\mathbf{I} - \mathbf{X}^2) = \mathbf{h} - \mathbf{f}\mathbf{h}^{-1}\mathbf{f}, \tag{A.5}$$

and some relations between determinants of them as

$$\det \boldsymbol{\gamma} = \det \mathbf{h} \det(\mathbf{I} - \mathbf{X}^2) = \det \mathbf{h}[\det(\mathbf{I} + \mathbf{X})]^2, \tag{A.6}$$

$$\det \mathbf{M} = \det \mathbf{h} \det(\mathbf{I} + \mathbf{X}) = \det \mathbf{h} \det(\mathbf{I} - \mathbf{X}). \tag{A.7}$$

As a result, we have

$$\det \mathbf{M} = \det \boldsymbol{\gamma}[\det(\mathbf{I} + \mathbf{X})]^{-1} \tag{A.8}$$

If the matrix $\mathbf{f}$ has rank 3, $\det(\mathbf{I} + \mathbf{X}) = 1 - \frac{1}{2}\mathrm{Tr}\mathbf{X}^2$.

The anti-symmetric part of $\mathbf{M}^{-1}$ is

$$\begin{aligned}(\mathbf{M}^{-1} - {}^t\mathbf{M}^{-1})/2 =& - \mathbf{h}^{-1}\mathbf{f}\mathbf{h}^{-1} - \mathbf{h}^{-1}\mathbf{f}\mathbf{h}^{-1}\mathbf{f}\mathbf{h}^{-1}\mathbf{f}\mathbf{h}^{-1} + \cdots \\ =& - (\mathbf{X} + \mathbf{X}^3 + \mathbf{X}^5 + \cdots)\mathbf{h}^{-1} \\ =& - \boldsymbol{\gamma}^{-1}\mathbf{f}\mathbf{h}^{-1} = -\mathbf{h}^{-1}\mathbf{f}\boldsymbol{\gamma}^{-1},\end{aligned} \tag{A.9}$$

Now, we will derive the equations of motion from the DBI action. Variation of the Lagrangian is

$$\begin{aligned}2\delta\sqrt{-\det M} =& \delta M_{ab}(M^{-1})^{ba}\sqrt{-\det M} = (\delta h_{ab} + \delta f_{ab})(M^{-1})^{ba}\sqrt{-\det M} \\ =& \left[(2g_{\mu\nu}(X)\partial_a X^\mu \partial_b \delta X^\nu + \partial_\nu g_{\alpha\beta}(X)\partial_a X^\alpha \partial_b X^\beta \delta X^\nu)(M^{-1})^{(ab)}\right. \\ & \left. -2\partial_a \delta a_b (M^{-1})^{[ab]}\right]\sqrt{-\det M}\end{aligned} \tag{A.10}$$

Using the formulas previously shown, the equations of motion are

$$\begin{aligned}-\partial_b(\omega\sqrt{-\gamma}g_{\mu\nu}(X)\gamma^{ab}\partial_a X^\mu) + \frac{1}{2}\omega\sqrt{-\gamma}\gamma^{ab}\partial_\nu g_{\alpha\beta}(X)\partial_a X^\alpha \partial_b X^\beta = 0, \\ 2\partial_a(\omega\sqrt{-\gamma}\gamma^{ab}f_{bc}h^{cd}) = 0\end{aligned} \tag{A.11}$$

As a result, we have

$$\begin{aligned}\hat{D}^2 X^\mu + \Gamma^\mu_{\alpha\beta}\hat{D}^a X^\alpha \hat{D}_a X^\beta + \hat{D}^a X^\mu \hat{D}_a \ln\omega = 0, \\ \hat{D}^a(\omega f_{ab}h^{bc}) = 0,\end{aligned} \tag{A.12}$$

where $\hat{D}_a$ denotes the covariant derivative with respect to $\gamma_{ab} \equiv h_{ab} + f_{ac}f_{bd}h^{cd}$ and $\omega \equiv [\det(\mathbf{I} - \mathbf{X})]^{-1/2} = (\det h/\det\gamma)^{1/4}$. Thus, we can regard γ_{ab} as an effective metric (up to a conformal factor).

Another Lagrangian giving us the above equations of motion can be constructed as

$$\begin{aligned}L[X, f, \gamma, h, \omega] =& \sqrt{-\gamma}\omega\left(\gamma^{ab}g_{\mu\nu}(X)\partial_a X^\mu \partial_b X^\nu + \frac{1}{2}f_{ac}f_{bd}\gamma^{ab}h^{cd} - \frac{1}{2}\gamma^{ab}h_{ab} - \frac{p-1}{2}\lambda_1\right) \\ & + \sqrt{-h}\omega^{-1}\lambda_2,\end{aligned} \tag{A.13}$$

where γ_{ab}, h_{ab} and ω are auxiliary fields. Since λ_1 and λ_2 are non-zero arbitrary constants, we can set $\lambda_1 = \lambda_2 = 1$ for simplicity.

B. $d \neq 0$ cases

In this appendix, we summarize equation of motions of the D7-brane for general cases with finite temperature and non-zero baryon number density ($d \neq 0$). We consider Schwarzschild-AdS$_5 \times S^5$ spacetime as the background solution:

$$ds^2 = \frac{-F(z)dV^2 - 2dVdz + d\vec{x}_3^2}{z^2} + d\phi^2 + \cos^2\phi d\Omega_3^2 + \sin^2\phi d\psi^2 \ , \quad F(z) = 1 - r_h^4 z^4 \ . \tag{B.1}$$

The bulk event horizon is located at $z = 1/r_h$ in this spacetime. Then, expression of the D7-brane action is the same as Eq. (3.2), except for components of the induced metric:

$$\begin{aligned} h_{uv} &= -Z^{-2}(FV_{,u}V_{,v} + V_{,u}Z_{,v} + V_{,v}Z_{,u}) + \Phi_{,u}\Phi_{,v} \ , \\ h_{uu} &= -Z^{-2}V_{,u}(FV_{,u} + 2Z_{,u}) + \Phi_{,u}^2 \ , \quad h_{vv} = -Z^{-2}V_{,v}(FV_{,v} + 2Z_{,v}) + \Phi_{,v}^2 \ . \end{aligned} \tag{B.2}$$

To eliminate f_{uv} from the action (3.2), we perform a Legendre transformation as

$$\begin{aligned} \hat{S} &\equiv S - \int dudv f_{uv}\frac{\delta S}{\delta f_{uv}} \\ &= -\mu_7 g_s^{-1} V_3 \Omega_3 \int dudv \Big[\Big(\frac{\cos^6\Phi}{Z^6} + d^2 \Big) \{ (h_{uv} + Z^2 \partial_u a_x \partial_v a_x)^2 \\ &\qquad - (h_{uu} + Z^2 \partial_u a_x^2)(h_{vv} + Z^2 \partial_v a_x^2) \} \Big]^{1/2} \ , \end{aligned} \tag{B.3}$$

where we have eliminated f_{uv} using Eq. (3.4) at the second equality. As well as the $d = 0$ case, we can impose the same coordinate conditions $C_1 \equiv h_{uu} + Z^2 \partial_u a_x^2 = 0$ and $C_2 \equiv h_{vv} + Z^2 \partial_v a_x^2 = 0$.

$$\hat{S} = \mu_7 g_s^{-1} V_3 \Omega_3 \int dudv \Big(\frac{\cos^6\Phi}{Z^6} + d^2 \Big)^{1/2} (h_{uv} + Z^2 \partial_u a_x \partial_v a_x). \tag{B.4}$$

From this action, we can obtain evolution equations for V, Z, Ψ and a_x, where $\Psi(u,v) \equiv \frac{\Phi(u,v)}{Z(u,v)}$. The evolution equations are written as

$$\begin{aligned} K_1 V_{,uv} &= \frac{3}{2} Z (Z\Psi)_{,u} (Z\Psi)_{,v} + \frac{3}{2} \tan(Z\Psi) \{ (Z\Psi)_{,u} V_{,v} + (Z\Psi)_{,v} V_{,u} \} \\ &\qquad + \frac{1}{2} K_3 V_{,u} V_{,v} + \frac{Z^3}{2} K_2 a_{x,u} a_{x,v} \ , \end{aligned} \tag{B.5}$$

$$\begin{aligned} K_1 Z_{uv} &= -\frac{3}{2} Z F (Z\Psi)_{,u} (Z\Psi)_{,v} + \frac{3}{2} \tan(Z\Psi) \{ (Z\Psi)_{,u} Z_{,v} + (Z\Psi)_{,v} Z_{,u} \} \\ &\quad - \frac{1}{2} K_3 (FV_{,u}V_{,v} + V_{,u}Z_{,v} + V_{,v}Z_{,u}) + \frac{1}{Z}(6 - K_2) Z_{,u} Z_{,v} - \frac{FZ^3}{2} K_2 a_{x,u} a_{x,v} \ , \end{aligned} \tag{B.6}$$

$$
\begin{aligned}
K_1\Psi_{,uv} = \frac{3}{2}\left(\Psi F + \frac{\tan(Z\Psi)}{Z}\right)(Z\Psi)_{,u}(Z\Psi)_{,v} \\
+ \frac{1}{2Z^2}\{K_2 - 3Z\Psi\tan(Z\Psi)\}\{(Z\Psi)_{,u}Z_{,v} + (Z\Psi)_{,v}Z_{,u}\} \\
+ \frac{\Psi}{2Z}\left(K_3 + \frac{3\tan(Z\Psi)}{Z^2\Psi}\right)(FV_{,u}V_{,v} + V_{,u}Z_{,v} + V_{,v}Z_{,u}) \\
- \frac{3\Psi}{Z^2}Z_{,u}Z_{,v} + \frac{FZ^2\Psi}{2}\left(K_2 - \frac{3\tan(Z\Psi)}{FZ\Psi}\right)a_{x,u}a_{x,v} \ , \qquad \text{(B.7)}
\end{aligned}
$$

$$
K_1 a_{x,uv} = \frac{3}{2}\tan(Z\Psi)\{(Z\Psi)_{,u}a_{x,v} + (Z\Psi)_{,v}a_{x,u}\} + \frac{1}{2Z}K_2(Z_{,u}a_{x,v} + Z_{,v}a_{x,u}) \ . \qquad \text{(B.8)}
$$

where functions K_1, K_2 and K_3 are defined as

$$
\begin{aligned}
&K_1 = 1 + d^2\frac{Z^6}{\cos^6(Z\Psi)} \ , \quad K_2 = 1 - 2d^2\frac{Z^6}{\cos^6(Z\Psi)} \ , \\
&K_3 = F_{,Z} - 5\frac{F}{Z} + d^2\frac{Z^6}{\cos^6(Z\Psi)}\left(F_{,Z} - 2\frac{F}{Z}\right) \ .
\end{aligned} \qquad \text{(B.9)}
$$

In general cases, conservation of the constraint equations is slightly modified as

$$
\partial_u\Big[\frac{1}{Z^2}\Big(\frac{\cos^6\Phi}{Z^6} + d^2\Big)^{1/2}C_2\Big] = \partial_v\Big[\frac{1}{Z^2}\Big(\frac{\cos^6\Phi}{Z^6} + d^2\Big)^{1/2}C_1\Big] = 0 \ . \qquad \text{(B.10)}
$$

C. Stark effect for scalar and vector mesons

In this section, we analytically examine shifts of spectra of scalar and vector mesons caused by a weak electric field, i.e. Stark effect. We focus only on homogeneous modes in (x_1, x_2, x_3) and s-modes of S^3. Then, the brane dynamics is described by $W(t,z) \equiv z^{-1}\sin\Phi(t,z)$ and $a_x(t,z)$. The first order static solution in the electric field E is given by

$$
\bar{W} = m + \mathcal{O}(E^2) \ , \qquad \bar{a}_x = -Et \ . \qquad \text{(C.1)}
$$

We consider the fluctuation of the static solution: $W(t,z) = \bar{W} + w$ and $a_x(t,z) = \bar{a}_x + a$. Hereafter, we set $m = 1$ to simplify the expression. Then, using the DBI action, up to the first order in E the quadratic action in the fluctuations $w(t,z)$ and $a_x(t,z)$ is simply written as

$$
S = \frac{1}{2}\int dt\int_0^1 dz\frac{1-z^2}{z}\Big[\dot{\chi}_+\dot{\chi}_- - (1-z^2)\chi'_+\chi'_- - 2iEz^2(\dot{\chi}_+\chi_- - \chi_+\dot{\chi}_-)\Big] \ , \qquad \text{(C.2)}
$$

where we have introduced complex fields, $\chi_\pm \equiv w \pm ia$ and omitted irrelevant overall factor of the DBI action. Decomposing the fields into Fourier modes as $\chi_\pm(t,z) = \int_{-\infty}^{\infty}d\omega\chi_\omega^\pm(z)e^{-i\omega t}$, we obtain decoupled equations of motion as

$$
\omega^2\chi_\omega^\pm = (\mathcal{H} \pm 4E\omega z^2)\chi_\omega^\pm \ , \quad \mathcal{H} \equiv -\frac{z}{1-z^2}\frac{d}{dz}\frac{(1-z^2)^2}{z}\frac{d}{dz} \ . \qquad \text{(C.3)}
$$

The eigenfunction e_n and eigenvalue ω_n^2 of the operator $\mathcal{H}$ is given by

$$e_n = N_n F(-n, -n-1, -2n-2; 1/z^2) \,, \qquad \omega_n^2 = 4(n+1)(n+2) \,, \qquad (n = 0, 1, 2, \cdots) \,, \tag{C.4}$$

where F is the Gaussian hypergeometric function and N_n is a normalization factor. Defining an inner product as $(f, g) \equiv \int_0^1 dz\, z^{-1}(1-z^2) f(z) g(z)$, we choose the normalization factor N_n so that $(e_n, e_m) = \delta_{mn}$ is satisfied. Thus, for $E = 0$, meson spectra are given by $\omega_n^{\pm} = 2\sqrt{(n+1)(n+2)}$ for both of the scalar and vector mesons [42]. The shifts of the eigenvalues in the presence of the weak electric field are given by $\delta\omega_n^{\pm} = \pm 2E(e_n, z^2 e_n)$. We can find $(e_n, z^2 e_n) = 1/2$ for any n. Therefore, we obtain

$$\delta\omega_n^{\pm} = \pm\frac{E}{m} \,, \tag{C.5}$$

where we restored the quark mass m. Note that shifts of spectra do not depend on the mode number n. So, the beat frequency also does not depend on n and is given by $\omega_{\rm beat} = \delta\omega_n^+ - \delta\omega_n^- = 2E/m$. This is consistent with our numerical calculation in section 6.1.

D. Error analysis

In this section, we estimate the error in our numerical calculations. We define absolute values of constraints as

$$\begin{aligned} C_u &\equiv | - V_{,u}(V_{,u} + 2Z_{,u}) + Z^2 (Z\Psi)_{,u}^2 + Z^4 a_{x,u}^2 | \,, \\ C_v &\equiv | - V_{,v}(V_{,v} + 2Z_{,v}) + Z^2 (Z\Psi)_{,v}^2 + Z^4 a_{x,v}^2 | \,. \end{aligned} \tag{D.1}$$

Analytically, they have to be exactly zero everywhere once we have imposed $C_u = 0$ and $C_v = 0$ at the initial surface and the AdS boundary. However, in actual numerical calculations, they become non-zero because numerical error does exist. To check constraint violation in terms of C_u and C_v is one of estimators of our numerical accuracy. Introducing integer N such that the mesh size is given by $\delta u = \delta v = \pi/(2N)$, we will see N dependence of the constraints. As explained in section 3, we use two numerical methods depending on whether before or after the intermediate surface. We will refer to the numerical method used after/before the intermediate surface as *method A/B*. Numerical domains for the method A and B are $\{(u, v) | 0 \leq v \leq u\}$ and $\{(u, v) | 0 \leq u - v \leq \pi/2, 0 \leq v \leq v_{\rm int}\}$, respectively.

As a typical example of the supercritical electric field, we choose the parameter as $E_f/m^2 = 1$ and $m\Delta V = 0.5$. In this case, the final state of the time evolution is a static black hole embedding and the effective horizon exists at the initial surface. Thus, we regard the initial surface as the intermediate surface and use only the method A. Figures 18(a), (b), (c) show C_u for $N = 400$, 800, 1600. We can see that they remain quite small (even for $N = 400$, we have $C_u < 10^{-6}$) and decrease as N

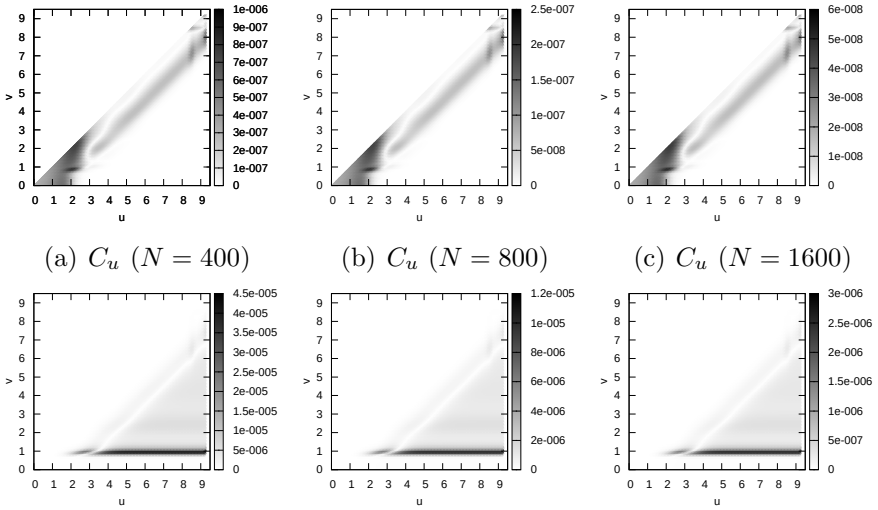

(a) C_u $(N = 400)$ (b) C_u $(N = 800)$ (c) C_u $(N = 1600)$

(d) C_v $(N = 400)$ (e) C_v $(N = 800)$ (f) C_v $(N = 1600)$

Figure 18: Constraint violation for $E_f/m^2 = 1$ and $m\Delta V = 0.5$.

increases. (See maximum values of color bars.) Figures 18(d), (e), (f) show C_v for $N = 400$, 800, 1600. They share a similar property as C_u.

As a typical example of the subcritical electric field, we choose the parameters as $E_f/m^2 = 0.19$ and $m\Delta V = 2$. In this case, the intermediate surface is located at $v = v_{\rm int} \simeq 5.5$, namely, numerical computation by the method B breaks down at $v = v_{\rm int}$. Figures 19(a)-(f) show C_u and C_v for $N = 400$, 800, 1600 before the intermediate surface. Although a sharp noise is generated at the pole on the initial surface and propagates between the AdS boundary and the pole, the constraint violation remains still small ($C_u, C_v < 3 \times 10^{-3}$ even for $N = 400$) and decreases as N increases. Figures 20(a)-(f) show C_u and C_v for $N = 400$, 800, 1600 after the intermediate surface. Our numerical calculation by the method A broke down at $u \simeq 3.6$. In the figures, we have focused on $3.5 \leq u \leq 3.6$ for C_u and $3.45 \leq u \leq 3.6$ and $0.3 \leq v \leq 0.45$ for C_v. The constraint violation localizes there because a singularity is close to the regions. We can find that the constraint violation remains still small ($C_u, C_v < 8 \times 10^{-3}$ even for $N = 400$) and decreases as N increases.

In section 6.2, we have inferred that a naked singularity appears on the brane for subcritical electric field case since the scalar quantity $s|_{\Phi=\pi/2} \equiv \gamma^{ab} h_{ab}|_{\Phi=\pi/2}$ seems to diverge within a finite time. We also found a turbulent-like behavior in brane fluctuations near the singularity. One may think that it is dangerous to treat a singularity by the numerical method and our results may be just numerical artifacts. Of course, we cannot "prove" the existence of the singularity from the numerical calculation. We can only show that our results do not depend on the resolution. Figure 21 shows the scalar quantity $s|_{\Phi=\pi/2}$ against the worldvolume coordinate v and the resolution N for $E_f/m^2 = 0.19$ and $m\Delta V = 2$. This figure demonstrates that the divergence of the scalar quantity does not depend on the resolution.

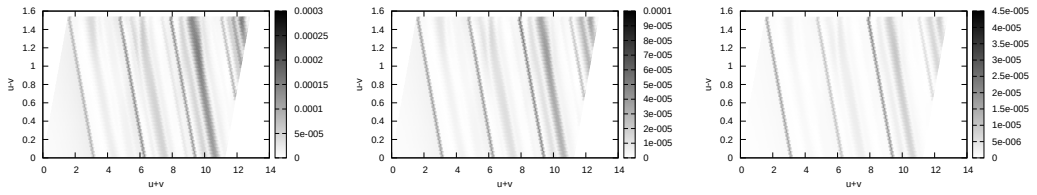

(a) C_u $(N = 400)$ (b) C_u $(N = 800)$ (c) C_u $(N = 1600)$

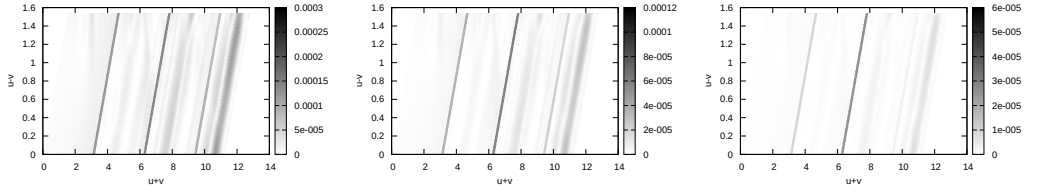

(d) C_v $(N = 400)$ (e) C_v $(N = 800)$ (f) C_v $(N = 1600)$

Figure 19: Constraint violation for $E_f/m^2 = 0.19$ and $m\Delta V = 2$ before the intermediate surface.

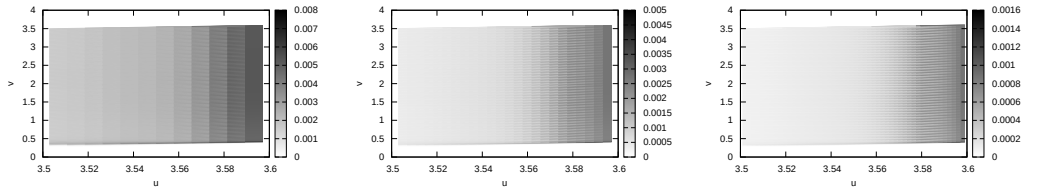

(a) C_u $(N = 400)$ (b) C_u $(N = 800)$ (c) C_u $(N = 1600)$

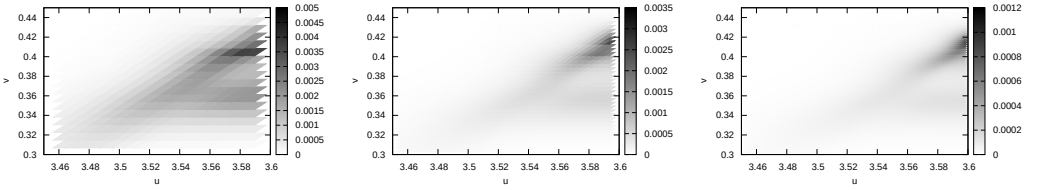

(d) C_v $(N = 400)$ (e) C_v $(N = 800)$ (f) C_v $(N = 1600)$

Figure 20: Constraint violation for $E_f/m^2 = 0.19$ and $m\Delta V = 2$ after the intermediate surface.

References

[1] D. E. Kharzeev, L. D. McLerran and H. J. Warringa, "The Effects of topological charge change in heavy ion collisions: 'Event by event P and CP violation'," Nucl. Phys. A **803**, 227 (2008) [arXiv:0711.0950 [hep-ph]].

[2] V. Skokov, A. Y. .Illarionov and V. Toneev, "Estimate of the magnetic field strength in heavy-ion collisions," Int. J. Mod. Phys. A **24**, 5925 (2009) [arXiv:0907.1396 [nucl-th]].

[3] V. Voronyuk, V. D. Toneev, W. Cassing, E. L. Bratkovskaya, V. P. Konchakovski and S. A. Voloshin, "(Electro-)Magnetic field evolution in relativistic heavy-ion collisions," Phys. Rev. C **83**, 054911 (2011) [arXiv:1103.4239 [nucl-th]].

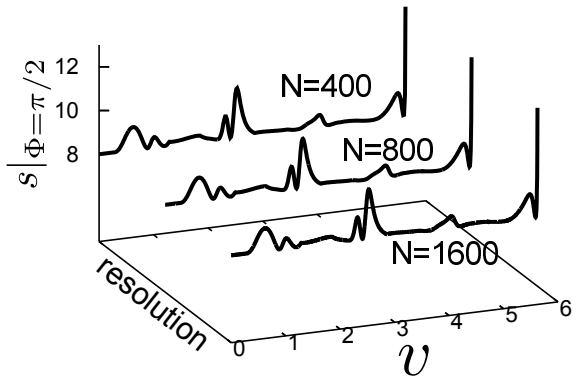

Figure 21: Resolution dependence of the scalar quantity $s|_{\Phi=\pi/2}$ for $E_f/m^2 = 0.19$ and $m\Delta V = 2$.

[4] A. Bzdak and V. Skokov, "Event-by-event fluctuations of magnetic and electric fields in heavy ion collisions," Phys. Lett. B **710**, 171 (2012) [arXiv:1111.1949 [hep-ph]].

[5] W. -T. Deng and X. -G. Huang, "Event-by-event generation of electromagnetic fields in heavy-ion collisions," Phys. Rev. C **85**, 044907 (2012) [arXiv:1201.5108 [nucl-th]].

[6] J. M. Maldacena, "The Large N limit of superconformal field theories and supergravity," Adv. Theor. Math. Phys. **2**, 231 (1998) [hep-th/9711200].

[7] S. S. Gubser, I. R. Klebanov and A. M. Polyakov, "Gauge theory correlators from noncritical string theory," Phys. Lett. B **428**, 105 (1998) [hep-th/9802109].

[8] E. Witten, "Anti-de Sitter space and holography," Adv. Theor. Math. Phys. **2**, 253 (1998) [hep-th/9802150].

[9] S. R. Das, T. Nishioka and T. Takayanagi, "Probe Branes, Time-dependent Couplings and Thermalization in AdS/CFT," JHEP **1007**, 071 (2010) [arXiv:1005.3348 [hep-th]].

[10] K. Hashimoto, N. Iizuka and T. Oka, "Rapid Thermalization by Baryon Injection in Gauge/Gravity Duality," Phys. Rev. D **84**, 066005 (2011) [arXiv:1012.4463 [hep-th]].

[11] T. Ishii, S. Kinoshita, K. Murata and N. Tanahashi, "Dynamical Meson Melting in Holography," JHEP **1404**, 099 (2010) [arXiv:1401.5106 [hep-th]].

[12] U. H. Danielsson, E. Keski-Vakkuri and M. Kruczenski, "Black hole formation in AdS and thermalization on the boundary," JHEP **0002**, 039 (2000) [hep-th/9912209].

[13] S. Bhattacharyya and S. Minwalla, "Weak Field Black Hole Formation in Asymptotically AdS Spacetimes," JHEP **0909**, 034 (2009) [arXiv:0904.0464 [hep-th]].

[14] R. A. Janik and R. B. Peschanski, "Gauge/gravity duality and thermalization of a boost-invariant perfect fluid," Phys. Rev. D **74**, 046007 (2006) [hep-th/0606149].

[15] H. Ebrahim and M. Headrick, "Instantaneous Thermalization in Holographic Plasmas," arXiv:1010.5443 [hep-th].

[16] J. Abajo-Arrastia, J. Aparicio and E. Lopez, "Holographic Evolution of Entanglement Entropy," JHEP **1011**, 149 (2010) [arXiv:1006.4090 [hep-th]].

[17] V. Balasubramanian, A. Bernamonti, J. de Boer, N. Copland, B. Craps, E. Keski-Vakkuri, B. Muller and A. Schafer *et al.*, "Thermalization of Strongly Coupled Field Theories," Phys. Rev. Lett. **106**, 191601 (2011) [arXiv:1012.4753 [hep-th]].

[18] A. Buchel, L. Lehner and R. C. Myers, JHEP **1208**, 049 (2012) [arXiv:1206.6785 [hep-th]].

[19] M. P. Heller, D. Mateos, W. van der Schee and D. Trancanelli, "Strong Coupling Isotropization of Non-Abelian Plasmas Simplified," Phys. Rev. Lett. **108**, 191601 (2012) [arXiv:1202.0981 [hep-th]].

[20] V. Balasubramanian, A. Bernamonti, J. de Boer, B. Craps, L. Franti, F. Galli, E. Keski-Vakkuri and B. Muller *et al.*, "Inhomogeneous Thermalization in Strongly Coupled Field Theories," Phys. Rev. Lett. **111**, 231602 (2013) [arXiv:1307.1487 [hep-th]].

[21] A. Buchel, L. Lehner, R. C. Myers and A. van Niekerk, "Quantum quenches of holographic plasmas," JHEP **1305**, 067 (2013) [arXiv:1302.2924 [hep-th]].

[22] A. Karch and E. Katz, "Adding flavor to AdS / CFT," JHEP **0206** 043 (2002), [arXiv:hep-th/0205236].

[23] A. Karch and A. O'Bannon, "Metallic AdS/CFT," JHEP **0709**, 024 (2007) [arXiv:0705.3870 [hep-th]].

[24] T. Albash, V. G. Filev, C. V. Johnson and A. Kundu, "Quarks in an external electric field in finite temperature large N gauge theory," JHEP **0808**, 092 (2008) [arXiv:0709.1554 [hep-th]].

[25] J. Erdmenger, R. Meyer and J. P. Shock, "AdS/CFT with flavour in electric and magnetic Kalb-Ramond fields," JHEP **0712**, 091 (2007) [arXiv:0709.1551 [hep-th]].

[26] K. Hashimoto and T. Oka, "Vacuum Instability in Electric Fields via AdS/CFT: Euler-Heisenberg Lagrangian and Planckian Thermalization," JHEP **1310**, 116 (2013) [arXiv:1307.7423].

[27] K. Hashimoto, T. Oka and A. Sonoda, "Magnetic instability in AdS/CFT : Schwinger effect and Euler-Heisenberg Lagrangian of Supersymmetric QCD," To be published in JHEP [arXiv:1403.6336].

[28] G. W. Semenoff and K. Zarembo, "Holographic Schwinger Effect," Phys. Rev. Lett. **107**, 171601 (2011) [arXiv:1109.2920 [hep-th]].

[29] J. Ambjorn and Y. Makeenko, "Remarks on Holographic Wilson Loops and the Schwinger Effect," Phys. Rev. D **85**, 061901 (2012) [arXiv:1112.5606 [hep-th]].

[30] S. Bolognesi, F. Kiefer and E. Rabinovici, "Comments on Critical Electric and Magnetic Fields from Holography," JHEP **1301**, 174 (2013) [arXiv:1210.4170 [hep-th]].

[31] Y. Sato and K. Yoshida, "Holographic description of the Schwinger effect in electric and magnetic fields," JHEP **1304**, 111 (2013) [arXiv:1303.0112 [hep-th]].

[32] Y. Sato and K. Yoshida, "Potential Analysis in Holographic Schwinger Effect," JHEP **1308**, 002 (2013) [arXiv:1304.7917, arXiv:1304.7917 [hep-th]].

[33] Y. Sato and K. Yoshida, "Holographic Schwinger effect in confining phase," JHEP **1309**, 134 (2013) [arXiv:1306.5512 [hep-th]].

[34] Y. Sato and K. Yoshida, "Universal aspects of holographic Schwinger effect in general backgrounds," JHEP **1312**, 051 (2013) [arXiv:1309.4629 [hep-th]].

[35] D. Kawai, Y. Sato and K. Yoshida, "The Schwinger pair production rate in confining theories via holography," arXiv:1312.4341 [hep-th].

[36] M. Sakaguchi, H. Shin and K. Yoshida, "No pair production of open strings in a plane-wave background," arXiv:1402.2048 [hep-th].

[37] A. S. Gorsky, K. A. Saraikin and K. G. Selivanov, "Schwinger type processes via branes and their gravity duals," Nucl. Phys. B **628**, 270 (2002) [hep-th/0110178].

[38] J. Sonner, "Holographic Schwinger Effect and the Geometry of Entanglement," Phys. Rev. Lett. **111**, 211603 (2013) [arXiv:1307.6850 [hep-th]].

[39] M. Chernicoff, A. Güijosa and J. F. Pedraza, "Holographic EPR Pairs, Wormholes and Radiation," JHEP **1310**, 211 (2013) [arXiv:1308.3695 [hep-th]].

[40] C. Barcelo, S. Liberati, S. Sonego and M. Visser, "Hawking-like radiation from evolving black holes and compact horizonless objects," JHEP **1102**, 003 (2011) [arXiv:1011.5911 [gr-qc]].

[41] S. Kinoshita and N. Tanahashi, "Hawking temperature for near-equilibrium black holes," Phys. Rev. D **85**, 024050 (2012) [arXiv:1111.2684 [hep-th]].

[42] M. Kruczenski, D. Mateos, R. C. Myers and D. J. Winters, "Meson spectroscopy in AdS / CFT with flavor," JHEP **0307**, 049 (2003) [hep-th/0304032].

[43] A. Karch and A. O'Bannon, "Holographic thermodynamics at finite baryon density: Some exact results," JHEP **0711**, 074 (2007) [arXiv:0709.0570 [hep-th]].

[44] S. Kobayashi, D. Mateos, S. Matsuura, R. C. Myers and R. M. Thomson, "Holographic phase transitions at finite baryon density," JHEP **0702**, 016 (2007) [hep-th/0611099].

[45] K. -Y. Kim, J. P. Shock and J. Tarrio, "The open string membrane paradigm with external electromagnetic fields," JHEP **1106**, 017 (2011) [arXiv:1103.4581 [hep-th]].

[46] S. Nakamura and H. Ooguri, "Out of Equilibrium Temperature from Holography," Phys. Rev. D **88**, 126003 (2013) [arXiv:1309.4089 [hep-th]].

[47] S. Nakamura, "Nonequilibrium Phase Transitions and Nonequilibrium Critical Point from AdS/CFT," Phys. Rev. Lett. **109**, 120602 (2012) [arXiv:1204.1971 [hep-th]].

[48] N. Seiberg and E. Witten, "String theory and noncommutative geometry," JHEP **9909**, 032 (1999) [hep-th/9908142].

[49] G. W. Gibbons and C. A. R. Herdeiro, "Born-Infeld theory and stringy causality," Phys. Rev. D **63**, 064006 (2001) [hep-th/0008052].

[50] G WGibbons, "Pulse propagation in Born-Infeld theory: The World volume equivalence principle and the Hagedorn - like equation of state of the Chaplygin gas," Grav. Cosmol. **8**, 2 (2002) [hep-th/0104015].

[51] G. Gibbons, K. Hashimoto and P. Yi, "Tachyon condensates, Carrollian contraction of Lorentz group, and fundamental strings," JHEP **0209**, 061 (2002) [hep-th/0209034].

[52] S. R. Das, D. A. Galante and R. C. Myers, "Universal scaling in fast quantum quenches in conformal field theories," Phys. Rev. Lett. **112**, 171601 (2014) [arXiv:1401.0560 [hep-th]].

[53] P. Bizon and A. Rostworowski, "On weakly turbulent instability of anti-de Sitter space," Phys. Rev. Lett. **107**, 031102 (2011) [arXiv:1104.3702 [gr-qc]].

[54] N. D. Birrell and P. C. W. Davis. "Quantum Fields in Curved Space," Cambridge University Press

[55] Y. Taguchi, T. Matsumoto, and Y. Tokura, "Dielectric breakdown of one-dimensional Mott insulators. Sr. 2CuO3 and SrCuO2," Phys. Rev. **B 62**, 7015 (2000).

[56] S. Iwai, M. Ono, A. Maeda, H. Matsuzaki, H. Kishida, H. Okamoto, and Y. Tokura, "Ultrafast optical switching to a metallic state by photo induced Mott transition in a halogen-bridged nuckel-chain compound," Phys. Rev. Lett. **91** 057401, (2003).

[57] S. Wall, D. Brida, S. R. Clark, H. P. Ehrke, D. Jaksch, A. Ardavan, S. Bonora, H. Uemura, Y. Takahashi, T. Hasegawa, H. Okamoto, G. Cerullo, and A. Cavalleri, "Quantum interference between charge excitation paths in a solid-state Mott insulator," Nat. Phys. **7**, 114 (2011).

[58] T. Suzuki and R. Shimano, "Exciton Mott Transition in Si Revealed by Terahertz Spectroscopy," Phys. Rev. Lett. **109**, 046402 (2012).

[59] T. Oka, R. Arita and P. Werner, "Breakdown of a Mott Insulator: A Nonadiabatic Tunneling Mechanism," Phys. Rev. Lett. **91** 066406, (2003).

[60] M. Eckstein, T. Oka, and P. Werner, "Dielectric Breakdown of Mott Insulators in Dynamical Mean-Field Theory," Phys. Rev. Lett. **105** 146404, (2010).

[61] T. Oka, "Nonlinear doublon production in a. Mott insulator: Landau-Dykhne method applied to an integrable model," Phys. Rev. **B 86** 075148 (2012).

[62] H. Aoki, N. Tsuji, M. Eckstein, M. Kollar, T. Oka, and P. Werner, "Nonequilibrium dynamical mean-field theory and its applications," to appear in Rev. Mod. Phys. , [arXiv:1310.5329[cond-mat]].

[63] T. Yoshioka and K. Asano, "Exciton-Mott Physics in a Quasi-One-Dimensional Electron-Hole System," Phys. Rev. Lett. **107** 256403, (2011).

[64] S. A. Moskalenko, D. W. Snoke, "Bose-Einstein Condensation of Excitons and Biexcitons", Cambridge Univ. Press (2000).

[65] M. Imada, A. Fujimori, and Y. Tokura, "Metal?insulator transitions," Rev. Mod. Phys. **70**, 1039 (1998).

[66] E. Brezin and C. Itzykson, "Pair Production in Vacuum by an Alternating Field," Phys. Rev. **D 2** 1191 (1970).

[67] V. S. Popov, JETP **34** 709 (1972).

[68] N. F. Mott, "The transition to the metallic state," Philos. Mag. **6**, 287 (1961).

[69] N. F. Mott, "Metal-Insulator Transition," Rev. Mod. Phys. **40**, 677 (1968).

[70] R. Zimmermann, K. Kilimann, W. D. Kraeft, D. Kremp, and G. Röpke, "Dynamical screening and self-energy of excitons in the electron?hole plasma," Phys. Status Solidi **B 90**, 175 (1978).